二维有机-无机杂化钙钛矿非线性光学研究进展 (特邀)

郑昀颢，韩　笑，徐加良

(南开大学 材料科学与工程学院，天津 300350)

摘　要：自从钙钛矿材料问世以来，有机-无机杂化钙钛矿材料在近数十年的时间得到了蓬勃发展。二维 (2D) 有机-无机杂化钙钛矿是由典型的无机八面体框架以及不同的有机阳离子构成，其具有本征的量子阱结构和有趣的光电特性，也因此在发光、传感器、调谐、光伏体系以及通讯设备等领域引起了人们的密切关注。低成本、可溶液法制备、以及可替换的有机阳离子等特性使二维杂化钙钛矿在光学和光子应用中具有灵活的层间距，层数和可变的晶格扭曲，从而实现可调节的框架以及在光学和光子学应用中的高调节度。尤其地，它们也表现出突出的二阶、三阶和高阶非线性光学特性，例如在激光脉冲激发下的二次谐波产生 (SHG)、太赫兹 、双光子吸收 (2PA) 和饱和吸收 (SA) 和三光子吸收 (3PA) 等。讨论了具有不同结构特点的二维杂化钙钛矿的构建，并重点介绍了这些二维杂化钙钛矿在线性和非线性光学领域地特性和应用。最后，对二维杂化钙钛矿的研究现状进行了评估，并对其未来发展进行了展望。

关键词：二维杂化钙钛矿；　量子阱结构；　结构可调性；　非线性光学

中图分类号：N93　　**文献标志码：**A　　**DOI：**10.3788/IRLA20201063

Recent progress in nonlinear optics of 2D organic-inorganic hybrid perovskites (*Invited*)

Zheng Yunhao，Han Xiao，Xu Jialiang

(School of Materials Science and Engineering, National Institute for Advanced Materials, Nankai University, Tianjin 300350, China)

Abstract: Since the advent of perovskite materials, the numerous organic-inorganic hybrid perovskites have thrived vigorously over the decades. Two-dimensional (2D) organic-inorganic hybrid perovskites containing prototypical inorganic octahedron frames and diverse organic cations feature characteristics of intrinsic quantum-well structures and intriguing optoelectronic properties, and have therefore attracted research attention intensively for their optical applications in light emitting, sensing, modulation, photovoltaic cells and telecommunication devices. The low-cost and solution-processed fabrications as well as the alternative organic spacer cations endue 2D hybrid perovskites with flexible layer distances, number of layers, and variable lattice distortion, leading to effectuate the adjustable frameworks as well as higher tunability in optical and photonic applications. In particular, they also demonstrate distinguished and appealing nonlinear optical (NLO) characters whether in the second-order, third-order NLOs or the higher-order NLOs such as second-harmonic generation (SHG), terahertz generation, two-photon absorption (2PA), and saturable absorption (SA), three-photon absorption (3PA), etc., under the excitation of laser pulses. Here, we discuss on the construction of the various 2D hybrid perovskites

收稿日期:2020−10−12；　**修订日期:**2020−11−25

基金项目:国家自然科学基金 (21773168)

作者简介:郑昀颢 (1999−)，男，本科生，主要从事晶态光学材料方面的研究工作。Email: 1343888138@qq.com

导师简介:徐加良 (1983−)，男，研究员，博士，主要从事光学功能材料研究。Email: jialiang.xu@nankai.edu.cn

with different structural features. Furthermore, some representative properties and applications of these 2D hybrid perovskites are discussed in both linear and nonlinear optical regimes. Lastly, the status quo and challenge of 2D hybrid perovskites are elevated, and the future developments of 2D hybrid perovskites is prospected.

Key words: 2D hybrid perovskites; quantum-well structure; structure tunability; nonlinear optics

0 引 言

自 2004 年单原子层状石墨烯问世以来[1], 二维材料的研究得到了高速发展[2]。此后, 过渡金属硫族化合物 (TMDs)[3−5]、石墨炔 (GD)[6−11]、六方氮化硼 (h-BN)[12−13]、黑磷 (BP)[14−15] 等新型二维材料凭借各自优异的化学和物理特性, 在光电子学[16]、光子学[17−20]、催化[21]、能量转换和存储材料[22, 23] 等领域大放异彩。

不仅如此, 这些二维材料很容易制备成相应的薄膜或纳米晶体, 被广泛应用于光子学研究。这与它们具有超大的比表面积[24]、优异的鲁棒性[25] 与机械灵活性[26]、高的表面灵敏度[27]、异质结构中的显著量子效应[28−29]、以及在范德华力作用下易堆叠[30] 等优点密不可分。

钙钛矿结构材料, 尤其是有机-无机杂化卤化钙钛矿, 具有制备成本低、性能优异的特点, 是一种高性能的半导体材料[31]。钙钛矿材料最具代表性的应用是作为性能优异的光伏材料[32−33], 在过去十年里极大地提高了光电转换效率[34]。当杂化钙钛矿材料的维度从三维降低到二维, 可以产生许多独特的性质, 如大的激子结合能 (>100 m*e*V)、较长的载流子扩散距离、优异的光吸收能力、可控的载流子迁移率和高效的光致发光强度[35−36]。在这些结构中, 重原子的引入与无机 [BX_6] 八面体的刚性结构的协同作用促进了材料室温磷光 (RTP) 和热激活延迟荧光 (TADF) 的产生[37]。另外, 可自由替换的有机配体和金属阳离子为钙钛矿材料提供了柔性的晶体结构、强大的抵抗性、可调带隙以及宽窄带发光的可能性。

非线性光学 (NLO) 研究物质与强光的强相互作用, 它的发展对现代技术如全光开关[38]、远程通信[39−40]、信息处理和存储[41−42] 等领域[43−45] 起着关键作用。当入射光通过介质时, 光与物质之间的相互作用会引起介质中电荷的相对位移, 在外加光场下产生极化 $\boldsymbol{P}(t)$, 其定义如下[46−47]:

$$\boldsymbol{P}(t)=\chi^{(1)}\boldsymbol{E}(t)+\chi^{(2)}\boldsymbol{E}(t)^2+\chi^{(3)}\boldsymbol{E}(t)^3+\cdots \quad (1)$$

式中: $\boldsymbol{E}(t)$ 代表外加光场的强度, $\chi^{(n)}$ 表示 n 阶极化率。$\chi^{(1)}$ 是线性光学极化率, 表现为在普通光, 如日照下的普通线性吸收、发射和折射[48]。非线性光学现象只能在激光等强光源下观察到[49−50]。强光所产生的极化作用可以诱导形成新的二次光场, 还会引起相位和频率的变化等[51], 因此, 非线性光学效应是光子调节技术和集成光路技术[52] 的关键, 对于未来的光通信和光计算等技术[53] 具有重要意义。

多种二维材料 (如石墨烯[54−56], 石墨炔[9, 57−59], TMDs[60−62], h-BN[63−64], BP[65−67], MOFs[68−70], COFs[71]) 均展现出优异的非线性光学效应。这些二维材料的出色非线性光学性能使其能够在频率转换、光整流、光调谐、光限幅和太赫兹生成及检测等许多重要领域中发挥作用。二维杂化钙钛矿材料的可极化性使其非常适用于非线性光学应用[53]。手性钙钛矿的研究极大推动了钙钛矿二阶非线性光学材料的发展[72]。为此, 笔者讨论了二维钙钛矿体系的结构特征, 总结了近年来它们在线性和非线性光学方面的主要研究进展, 并对二维杂化钙钛矿非线性光学材料的研究现状及面临的挑战进行了分析。

1 二维钙钛矿的结构

最早发现的钙钛矿 $CaTiO_3$ 属于 ABX_3 型的三维钙钛矿体系。通常 A 为小的有机或无机阳离子, B 为过渡金属阳离子 (如 Pb^+, Sn^{2+}或 Ag^+), X 为卤素阴离子 (Cl^-, Br^-或 I^-), 其基元为顶角共享的 [BX_6] 八面体[73−74]。通常 ABX_3 钙钛矿的构造遵循 Goldschmidt 公差因子, 该因子决定了阳离子半径约为 2.6 Å才能保证钙钛矿稳定的刚性三维骨架[75−76]。进一步的探索表明, 阳离子 A 的细微变化将引起钙钛矿材料的结构、形态甚至尺寸的变化[77]。而当 Goldschmidt 公差因子 t >1 时, 标准三维骨架很难成形, 只能转换为低维 (二维, 1D, 0D) 钙钛矿材料。

具有分子式 $R_2A_{n-1}B_nX_{3n+1}$(R 代表额外的大体积有机阳离子) 的二维杂化钙钛矿[78] 可以看作是从标准三维钙钛矿切割下来的子结构。通过沿不同的晶体学取向将三维框架切割, 可以将二维层状钙钛矿分为 (100), (110) 和 (111) 衍生物 (图 1)[79]。反之, 通过增加钙钛矿层的数量 (n 的值) 也可实现从纯二维钙钛矿到准二维钙钛矿再到三维钙钛矿的转化 (图 2)[80−81]。

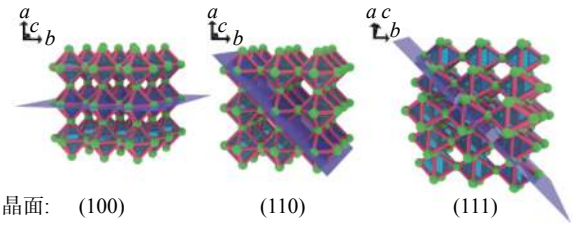

图 1 通过沿着晶体学平面 (100), (110) 和 (111) 切割经典的三维层状卤化钙钛矿的立方晶格衍生得到二维卤化钙钛矿

Fig.1 Derivation of 2D halide perovskites from the parental cubic perovskite lattice of 3D layered halide perovskites by cutting the latter along typical crystallographic planes: (100), (110), and (111)

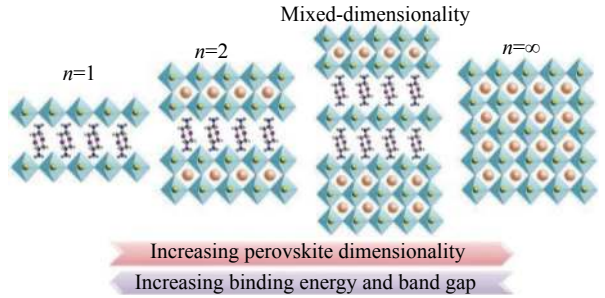

图 2 二维钙钛矿 (n = 1 和 2, 其中 n 代表金属卤化物晶格), 混维钙钛矿和三维钙钛矿 (n =∞) 的晶体结构示意图[80]

Fig.2 Schematic illustration showing the crystalline structure of 2D perovskites (n = 1 and 2, where n represents the metal halide lattices), mixed-dimensionality perovskites and 3D perovskites (n = ∞)[80]

1.1 (100) 类二维钙钛矿

从结构上讲, (100) 钙钛矿衍生物主要可分为 R-P (Ruddlesden-Popper) 相[82−83], D-J(Dion-Jacobson) 相[84−86] 和 ACI 相[87−88] 层状钙钛矿, 其特征通式分别为 $A'_2A_{n-1}B_nX_{3n+1}$, $A'A_{n-1}B_nX_{3n+1}$ 和 $A'A_nB_nX_{3n+1}$。这三种类型的二维钙钛矿之间的主要区别是无机组分堆积模式的不同。在 (a, b) 层平面中, D-J 相相邻的无机双层采用更均匀的堆叠模式, 表现出 (0, 0) 的面内位移[89]。而在 R-P 相和 ACI 相中可以观察到相对交错的堆叠模式, 分别表现出 (0.5, 0.5) 和部分 (0.5, 0) 位移[86]。R-P 相钙钛矿要求一对一价间隔阳离子插入每个八面体单元的夹层中 (图 3), 而 D-J 相对应物只需

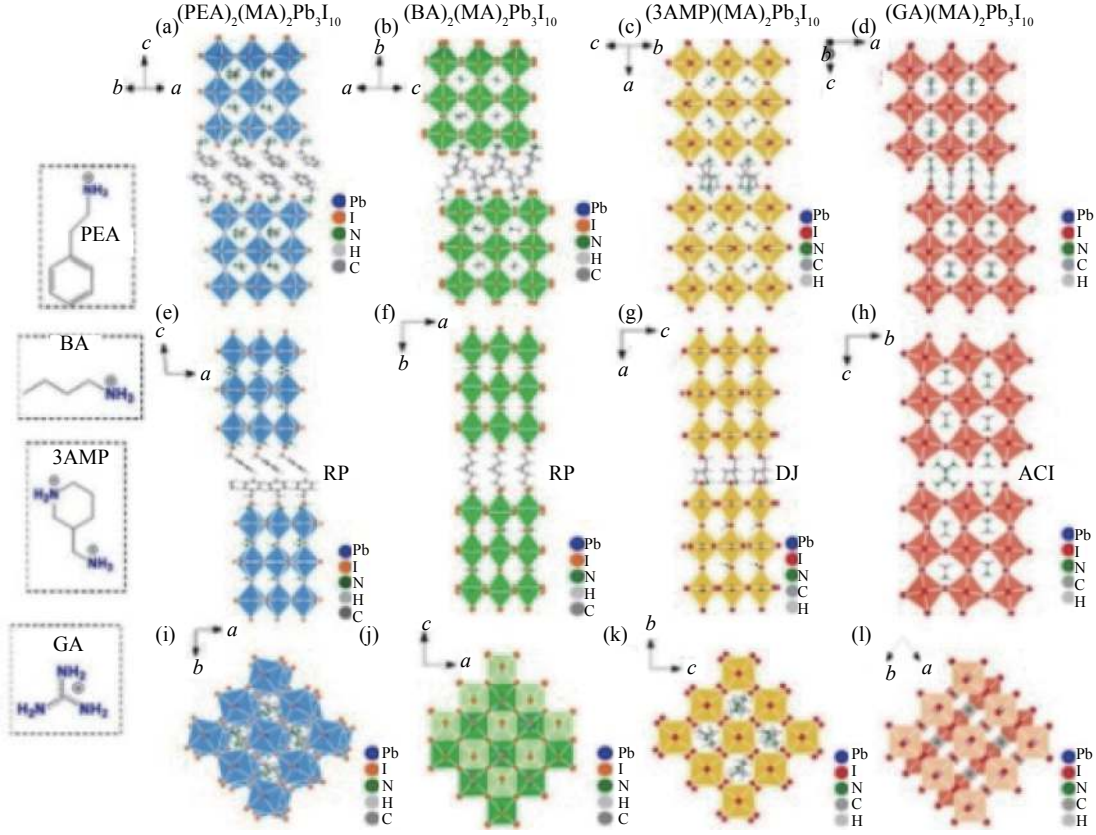

图 3 R-P 相, D-J 相和 ACI 相二维钙钛矿的 n = 3 晶体结构比较: (A, E, I) $(PEA)_2(MA)_2Pb_3I_{10}$; (B, F, J) $(BA)_2(MA)_2Pb_3I_{10}$; (C, G, K) $(3AMP)_2(MA)_2Pb_3I_{10}$; (D, H, L) $(GA)(MA)_3Pb_3I_{10}$[89]

Fig.3 Structural comparison among the n = 3 crystal structures of the R-P phase, D-J phase, and ACI phase 2D perovskites: (A, E, I) $(PEA)_2(MA)_2Pb_3I_{10}$; (B, F, J) $(BA)_2(MA)_2Pb_3I_{10}$; (C, G, K) $(3AMP)_2(MA)_2Pb_3I_{10}$; and (D, H, L) $(GA)(MA)_3Pb_3I_{10}$[89]

要一个二价间隔阳离子。在 R-P 钙钛矿中，无机立方层可以更灵活、更自由地堆叠，因此其分子间的相互作用较弱。而层间间距的细微变化会对钙钛矿的光电性能产生极大的影响。例如，Iwan 等人报道了基于对称的 Bn (苯并咪唑鎓) 和 Bdi (苯并二咪唑鎓) 阳离子的含锡钙钛矿[90]。Bdi^{2+}阳离子中的两个咪唑环同时与上下层相互作用 (图 4(a))，将 Bn_2SnI_4 的层间距 13.95 Å(1 Å=10^{-10}m) 压缩为 $BdiSnI_4$ 的 10.59 Å (图 4(b))。

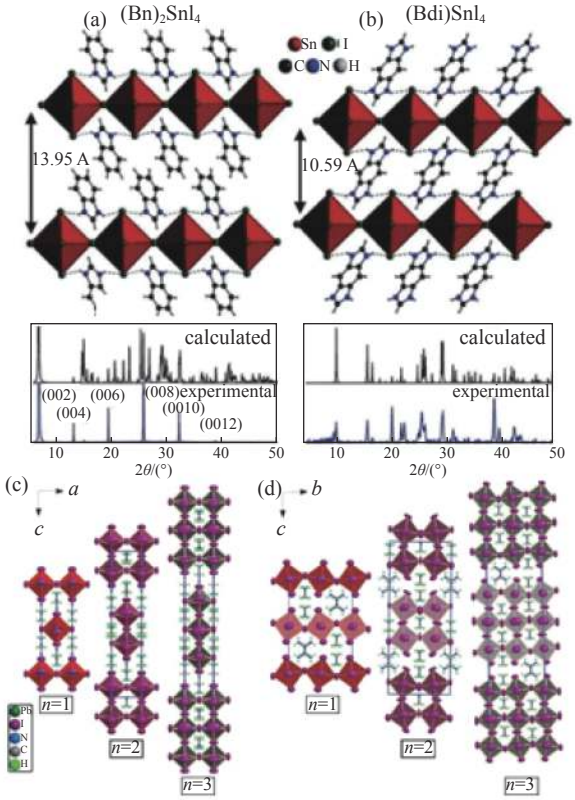

图 4 垂直于堆叠方向的二维钙钛矿 $[benzimidazolium]_2SnI_4$ (a) 和 $[benzodiimidazolium]SnI_4$(b) 的结构图。单个钙钛矿片之间的 *d* 间距已标出。下方显示了旋涂在玻璃基板上的二维钙钛矿的相应衍射图样[90]。$(GA)(MA)_nPb_nI_{3n+1}$ (n = 1−3) 钙钛矿的晶胞沿 (c) 结晶 *b* 轴和 (d) 结晶 *a* 轴的视图[88]

Fig.4 Structural drawings of the 2D perovskites $[benzimidazolium]_2SnI_4$ (a) and $[benzodiimidazolium]SnI_4$ (b) Perpendicular to the stacking direction. The *d*-spacing between the single perovskite sheets indicated. The corresponding diffraction patterns of the 2D perovskites spin-coated on glass substrates are shown underneath[90]. View of the unit cells of the $(GA)(MA)_nPb_nI_{3n+1}$ (n = 1−3) perovskites along (c) Crystallographic *b*-axis and (d) Crystallographic *a*-axis highlighting the ordered crystal packing of the GA and MA cations between the perovskite layers[88]

与 $BdiMI_4$ 相比，这种层间间距的变化导致 Bn_2MI_4 晶体沿 (001) 方向优先生长，同时使得其电导率下降。

类似地，Li 等人提出了两种二维 D-J 相卤化物钙钛矿 $(4AMPY)(MA)_{n-1}Pb_nI_{3n+1}$ 和 $(3AMPY)(MA)_{n-1}Pb_nI_{3n+1}$ (MA =甲基铵，4AMPY = 4−(氨基甲基) 吡啶，3AMPY = 3−(氨基甲基) 吡啶)。更短的层间距使得 $(3AMPY)(MA)_{n-1}Pb_nI_{3n+1}$ 钙钛矿的带隙更窄，通过量子阱结构容易分离的电子-空穴对使芳香族体系的激子结合能 (E_b) 变小[91]。

除了层间距之外，钙钛矿光电性能也与它们的层数和晶格扭曲密切相关。与三维结构钙钛矿相比，二维或准二维钙钛矿具有更大的 E_g 和更高的 E_b，此外，二维平面中的量子限域效应和表面钝化提高了光致发光量子产率 (PLQY)[92−94]。当 $n \geqslant 2$ 时，随 n 值增大逐渐组装的无机八面体层形成了所谓“阱”[95]。

在 ACI 型钙钛矿 $(C(NH_2)_3)(CH_3NH_3)_nPb_nI_{3n+1}$ 中，其光学带隙在同一体系中随着层间距的改变呈单调性变化[88]。有趣的是，当层数为奇数 (n = 1、3) 时，该 ACI 钙钛矿属于中心对称 *Imma* 空间群；而层数为偶数 (n = 2) 时，则体系属于非中心对称的 *Bmm2* 空间群 (图 4(c)、(d))。这种变化源自晶体对称性因子的变化，n 取偶数时出现镜面对称，n 取奇数时出现滑移面。Yuan 等人通过控制层厚 n 和纳米级杂化层状卤化物钙钛矿中的有机阳离子来调节发光颜色[96]。利用反胶束一锅法，层数 n 从 1 增加到无穷大，实现了其光致发光从深蓝色到绿色的红移。

通常八面体 B-X-B 二面角可估计晶格扭曲效应，较大的二面角通常对应于晶体骨架的较小扭曲[89, 97]。虽然钙钛矿晶格中的结构变形不如中间层对系统的影响大[89]，但它在调节钙钛矿材料的性能方面仍然发挥着不可估量的作用。例如，由瞬态晶格扭曲产生的自陷激子 (STE) 会导致强烈的 Stokes 位移和超能带发射[97−99]。

最近，Jung 等人制备了 $(BZA)_2PbBr_{4-x}Cl_x$ (BZA = 苄基胺，x = 0, 1.5, 2, 3, 3.5, 4)，用于可调式固态发光[100]。钙钛矿 $(BZA)_2PbBr_4$ 和 $(BZA)_2PbCl_4$ 分别发出窄的蓝光和蓝绿光 (图 5(a)、(b))。对比不同的无机层的结构数据，相邻八面体的 Pb-Br-Pb 二面角几乎相同 (149.9°和 150.0°)(图 5(c))，而 Pb-Cl-Pb 结合角急剧变化 (142.2°和 154.4°)(图 5(d))。$(BZA)_2PbCl_4$ 的较大变形

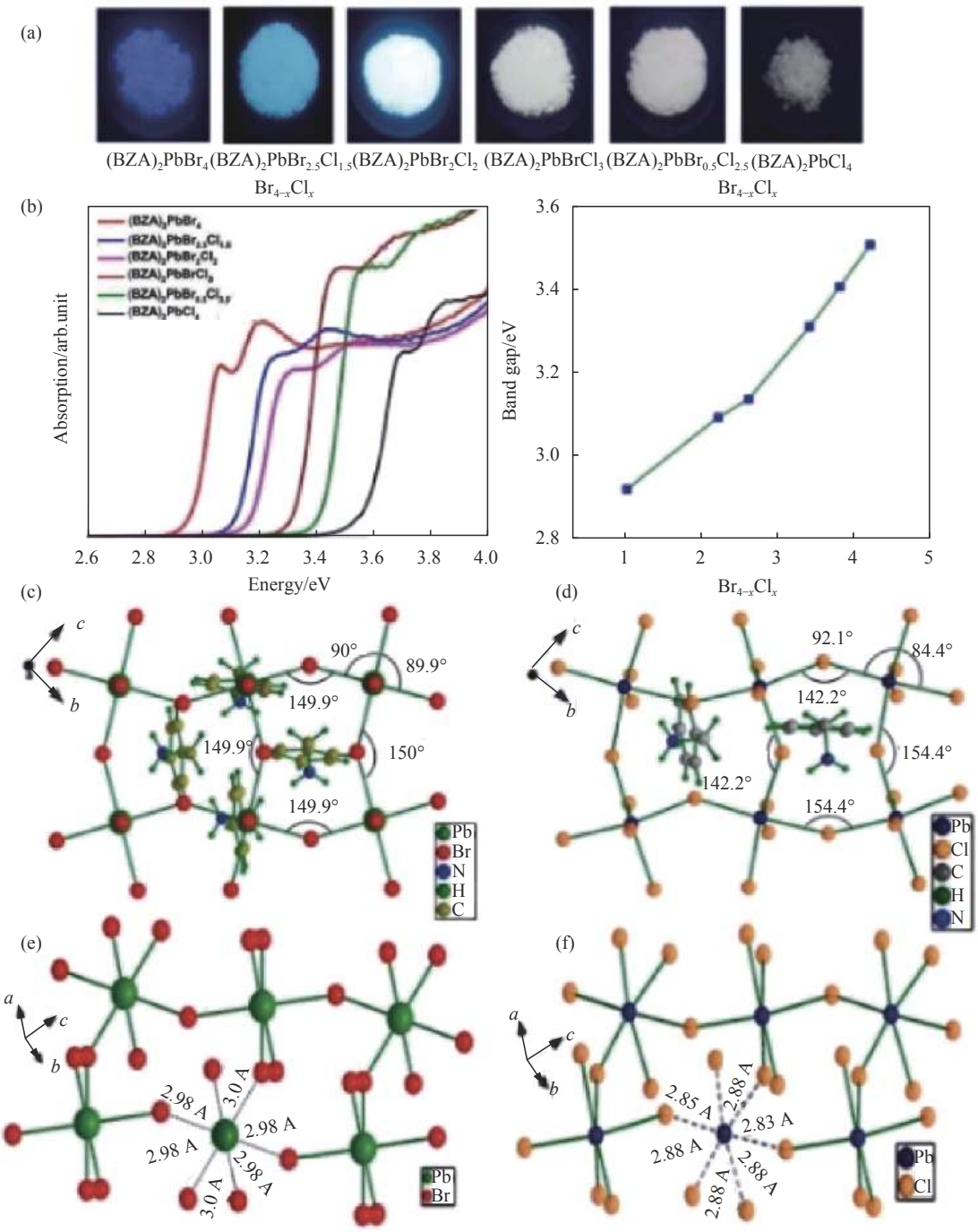

图 5 (a) 在紫外线激发下 $(BZA)_2PbBr_4$ 粉状多晶样品的蓝光发射和 $(BZA)_2PbBr_{4-x}Cl_x$ (x = 1.5, 2, 3, 3.5, 4) 钙钛矿系列的白光发射。λ_{ex} = 365 或 254 nm; (b) $(BZA)_2PbBr_{4-x}Cl_x$ 钙钛矿 (x = 4, 3.5, 3, 2, 1.5, 0) 系列固体粉末的漫反射光谱和带隙; (c) $(BZA)_2PbBr_4$; (d)$(BZA)_2PbCl_4$ 的几何结构。$PbBr_6^{2-}$和 $PbCl_6^{2-}$八面体的 Pb-Br 键距 (e) 和 Pb-Cl 的键距 (f)[100]

Fig.5 (a) Blue-light emission from $(BZA)_2PbBr_4$ powdered polycrystalline sample and white-light emission from the $(BZA)_2PbBr_{4-x}Cl_x$ (x = 1.5, 2, 3, 3.5, 4) perovskite series under UV excitation at λ_{ex} = 365 or 254 nm; (b) Diffuse reflectance spectra and band gaps of the solid powder of the $(BZA)_2PbBr_{4-x}Cl_x$ perovskite (x = 4, 3.5, 3, 2, 1.5, 0) series. Structural geometry of (c) $(BZA)_2PbBr_4$ and (d) $(BZA)_2PbCl_4$. Bond distances of (e) Pb−Br and (f) Pb−Cl for $PbBr_6^{2-}$ and $PbCl_6^{2-}$octahedra, respectively[100]

导致宽带发射。类似地，Zou 等人报道了杂化钙钛矿 $(C_6H_5C_2H_4NH_3)_2PbBr_4$ 在不同压力下结构转变造成的宽带发射[101]。这在制造超高压环境中的光电探测器方面具有潜在价值。

1.2 其他二维钙钛矿衍生物

(110) 取向的钙钛矿衍生物在三种类型的二维钙钛矿衍生物中相对较少，因为很少存在有机阳离子能够稳定该二维骨架。尽管如此，(110) 取向的钙钛矿衍生物中的主要氢键相互作用可以同时起到稳定二维钙钛矿结构和影响生长的作用[102]。在可延展的无机骨架中，特殊的有机阳离子堆积促进了 (110) 取向钙钛矿扭曲结构的形成。实际上，(110) 型钙钛矿是二维钙钛矿中弯曲度最高的钙钛矿衍生物，它们通式为 $A'_2A_mB_mX_{3m+2}$，具有屋脊型的层式结构[103]。以屋脊型八面体晶格的“屋脊长度”为分类标准，(110) 取向钙钛矿可分为“2×2”，“3×3”和“4×4”三个系列 (图 6(b))[104−105]。由于 STEs 效应，(110) 取向钙钛矿的高度扭曲结构使它们在室温下即具有宽带发射效应[106−108]。

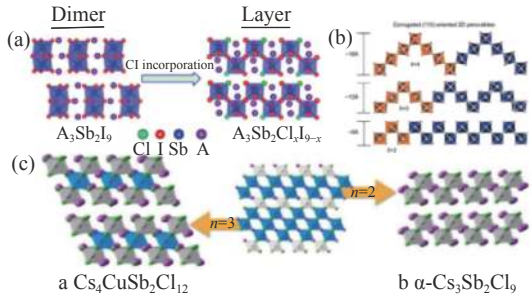

图 6 (a) 从 $A_3Sb_2I_9$ 的 0 维二聚体相到 $A_3Sb_2Cl_xI_{9-x}$.的二维层状相的 Cl 加成诱导转变示意图[104]; (b) 二维钙钛矿各族波纹状 (110) 取向排列的不同结构类型示意图[110]; (c) 具有通式 $A_{n+1}B_nX_{3n+3}$ 的 (111) 取向钙钛矿家族，可以通过沿三维母体结构的 (111) 方向切割而获得; (a) 和 (b) 显示 $Cs_4CuSb_2Cl_{12}$ 和 α-$Cs_3Sb_2Cl_9$ 的晶体结构。绿色和紫色的球体分别代表 Cl 和 Cs 原子; 灰色和蓝色分别代表 Sb 和 Cu 配位多面体[112]

Fig.6 (a) Schematic plot of the Cl-addition-induced transformation from the 0D dimer phase of $A_3Sb_2I_9$ to the 2D layered phase of $A_3Sb_2Cl_xI_{9-x}$[104]; (b) Schematic representation of different structural types of corrugated (110)-oriented members of the 2D perovskite family[110]; (c) (111)-oriented perovskite family with general formula, $A_{n+1}B_nX_{3n+3}$, which can be obtained by cutting along the (111)-direction of the 3D parent structure. Panels (a) and (b) show the crystal structures of $Cs_4CuSb_2Cl_{12}$ and α-$Cs_3Sb_2Cl_9$. Cl and Cs atoms are depicted as green and purple spheres, respectively; Sb and Cu coordination polyhedra are shown in gray and blue, respectively[112]

(111) 取向的钙钛矿可用通式 $A'_2A_{k-1}B_kX_{3k+3}$ 表示，可以认为是三维钙钛矿沿体对角线分裂而形成，这造成了 M 位的缺陷[89, 109]。$A'_2A_{k-1}B_kX_{3k+3}$ 族由一价阳离子 (R-NH_3^+, Cs^+, Rb^+) 和 VA 族元素 B (As^{3+}, Sb^{3+}, Bi^{3+}) 组成。它自发形成二维的角共享的分层钙钛矿 (k=2) 或零维的面共享二聚体簇 (k=1)，以稳定 $(B_2X_9)^{3-}$ (图 6(a)) 的立体构型并实现电荷平衡[110−111]。值得注意的是，当 k> 2 时，参与 $A'_2A_{k-1}B_kX_{3k+3}$ 构造的 B 阳离子应处于分数价态或不同价态的混合体。最近，Brenda Vargas 合成了一个 (111) 取向的二维钙钛矿 $Cs_4Cu^{I}Sb^{III}_2Cl_{12}$, ($k$ = 3)[112]，由角共享的 $[CuCl_6]$ 和 $[SbCl_6]$ 晶胞共同构成了主要骨架 (图 6(c))。

获取二维钙钛矿的柔性结构[113]需借助可控的合成方法，它们固有的弱离子键将起到决定性作用[114]。二维杂化钙钛矿的主要制备方法可分为溶液法和气相法[115]。通常，溶液方法具有多种优点，其处理过程十分经济，可以很容易通过改变溶液系统来获取钙钛矿的多种形态。2015 年，Dou 等人通过溶液晶体生长法制备了 $(C_4H_9NH_3)_2PbBr_4$ 二维超薄杂化钙钛矿[36]。借助三元溶剂系统 (DMF，氯苯和乙腈)，在基板上结晶出均匀二维片状材料，其最小厚度约为 1.6 nm。Li 等人研究了掺入 Cl 的浓度对 $(BA)_2SnI_xCl_{4-x}$ (BA = n−$CH_3CH_2CH_2CH_2NH_3$) 钙钛矿的形貌、晶相和光学性质的影响[116]。随着 Cl 剂量的增加，二维钙钛矿的形态从片状转变为针状。同时，样品的发射峰呈现红移，相变温度也因较高的含 Cl 比而产生了急剧变化。

气相法可分为化学气相沉积法 (CVD)[117]和范德华力外延法 (van der Waals epitaxy)。尽管气相法通常价格昂贵并且需要较高的温度，但它们适用于合成具有更好的结晶度和更高纯度的二维钙钛矿。Chen 等人结合溶液法和 CH_3NH_3Br 的 CVD 来合成二维同源钙钛矿 $(BA)_2(MA)_{n-1}Pb_nBr_{3n+1}$[118]，所得的超薄大尺寸钙钛矿表现出优异的光电响应特性和出色的稳定性。Shi 等人报道了通过范德华外延生长的高质量 $(C_4H_9NH_3)_2PbI_4$ 薄片，由于范德华相互作用，晶体厚度变薄，电子-声子耦合强度降低[119]。

2 光学性质和应用

由于引入了较大的有机阳离子，钙钛矿的原有三维结构排列受到破坏[120]，最初的无机框架被向外延

伸的有机阳离子双层夹在中间[121], 给无机层带来了更高的电荷载流子迁移率和可调节的带隙[122−123]。因此, 与三维同源物相比, 二维杂化有机-无机钙钛矿表现出低介电系数和强激子结合能[114]。此外, 有机组分在溶液加工过程中的可扩展性和可替换性也使二维钙钛矿具有了多种多样的优异光学性能和应用[94, 124−125]。

2.1 二维钙钛矿的线性光学性质

室温下的光致发光[126]是二维层状钙钛矿的重要光学现象, 其本质是激子的辐射复合[127]。激子的自定域化加大了 Stokes 频移并扩大了宽带发光的范围, 使二维钙钛矿成为应用于发光二极管[128−129], 太阳能电池[130−131]和光电探测器[132−133]的重要材料。

2014 年初, Karunadasa 等人合成了一系列二维激发白光层状钙钛矿 (EDBE)[PbX_4](EDBE = 2, 2′-(乙二氧基) 双 (乙基铵); X = Cl, Br, I), 光致发光量子效率 (PLQEs) 增长到 9%[134]。恒定且稳定的辐射维持了三个月。对晶体结构的研究表明, 由激子耦合产生的晶格变形和固有的自陷效应有助于连续且宽泛的白光发射[135−136]。根据此原理, 可得到一系列二维杂化钙钛矿 $(C_6H_5C_2H_4NH_3)_2PbCl_4$[137],$(CH_3CH_2NH_3)_4Pb_3Br_{10-x}Cl_x$[138], $(C_4H_9NH_3)_2PbCl_4$[139], 和 (3APr)PbX_4 (3APr = 3−氨基吡咯烷鎓)[102], 并实现了室温条件下显著的白光发射。

长余辉发光材料一直被广泛关注, 并在传感器、存储和安全领域中展现了潜在的应用价值[140]。此外, 用于 RTP 发光体的系间窜越 (ISC) 过程和用于 TADF 发光体的反系间窜越 (RISC) 过程使得内量子效率 (IQE) 可达 100%[141]。Yan 等人开发出基于 Cd 的杂化卤化物二维钙钛矿 $CdCl_2$-4HP(4HP = 4−羟基吡啶) 的特殊 D-π-A 结构, 其在 416 nm 处有延迟荧光, 寿命长达 103.12 ms (图 7(c) 和 7(d))[37]。量子限域效应、恰到好处的重原子效应和刚性层状结构 (图 7(a)), 造就了罕见的深蓝色光发射 (图 7(b)) 和高的发射效率 (63.55%)。类似地, Hu 等人观察到的新型二维钙钛矿 $(PEA_{1-x}TTMA_x)_2PbBr_4$ (PEA = 苯乙铵, TTMA = 噻吩并 [3, 2-b] 噻吩-2-甲基铵) 的磷光, 寿命为 0.2 ms, 在室温下磷光产率为 11.2%[142]。因为从三重态 (T_1) 到基态 (S_0) 的转变是禁阻的, TTMA 有机分子在室温下不发磷光[143]。但是, 当将 TTMA 有机分子插入钙钛矿的无机骨架中时, 在无机组分中收集的能量转移到 TTMA, 就可以引发磷光。进一步的研究表明, 混合阳离子将主客体系统用于钙钛矿可以有效地抑制非辐射复合, 从而提高磷光寿命和量子产率[144−145]。

钙钛矿中可替换的有机物阳离子不仅可以改变其带隙、发光颜色[142]、寿命、稳定性[146]和效率[147], 而且还带来了新的光学性质。例如, 当把手性有机物引入钙钛矿骨架中时, 原始的几何中心对称性将被破坏。结果可以检测到圆二色性 (CD) 和圆偏振光 (CPL) 响应。2018 年, Xu 等人通过将手性胺结合到钙钛矿晶体结构中, 报道了一种手性钙钛矿 $(MPEA)_{1.5}PbBr_{3.5}(DMSO)_{0.5}$[148]。其晶体结构表明, 部分取代 Br 的 DMSO 溶剂分子插层于部分边共享的无机层的面上并与 Pb^{2+}形成配位 (图 7(e))。旋涂制备 *R*-和 *S*-$(MPEA)_{1.5}PbBr_{3.5}(DMSO)_{0.5}$ 薄膜, 发现二者均在 325 和 405 nm 光处表现出强烈的 CD 信号响应 (图 7(g))。此外, 通过在相同的三元溶剂系统中进行液体扩散而生长的纳米线型晶体, 隶属于相同的三斜晶系 *P*1 空间群。根据漫反射光谱, 计算出光学带隙约为 3.07 eV, 同时, 所制备出来的钙钛矿纳米线在 400 nm 光的刺激下显示了宽的包括整个可见光区域的发射范围 (图 7(f))。该纳米线型晶体发射的色度坐标为 (0.40, 0.42), 即发出暖淡黄白光。

2018 年, Long 等人报道了手性二维钙钛矿中没有环境磁场的情况下 3% 的自旋极化光致发光[125], 在传统三维钙钛矿中, 该现象只有在 5T 的磁场下才能实现。在该手性二维钙钛矿中, 手性配体 (*R*-/*S*-甲基苄基溴化铵) 的引入 (n = 2) 使得 CD 光谱中表现出明显的旋光性以及高效的 CPL 发光。此外, 钙钛矿对映体的外消旋体的极化程度随外部磁场线性变化, 实现了非手性钙钛矿的自旋控制。

近来, Li 等人在 57%HI 溶液中, 通过简便的溶液合成, 无需退火制备得到橙色针状手性钙钛矿 *R*/*S*-*α*-$(PEA)_2PbI_4$[149]。比较其左旋光 (σ^-) 和右旋光 (σ^+), 可发现在大约 500 nm 处的圆偏振光发射强度出现了显著的差异 (图 7(h),(I)), 这表明这对手性钙钛矿对映体具有高效的发光选择性。将该手性钙钛矿进一步应用于 CPL 检测中, 显示了出色的可重复性和光开关特性 (图 7(j)), 并且展现了超高的外部量子效率 (接近 140%)。

除通用的发光材料外, 二维杂化钙钛矿还与很

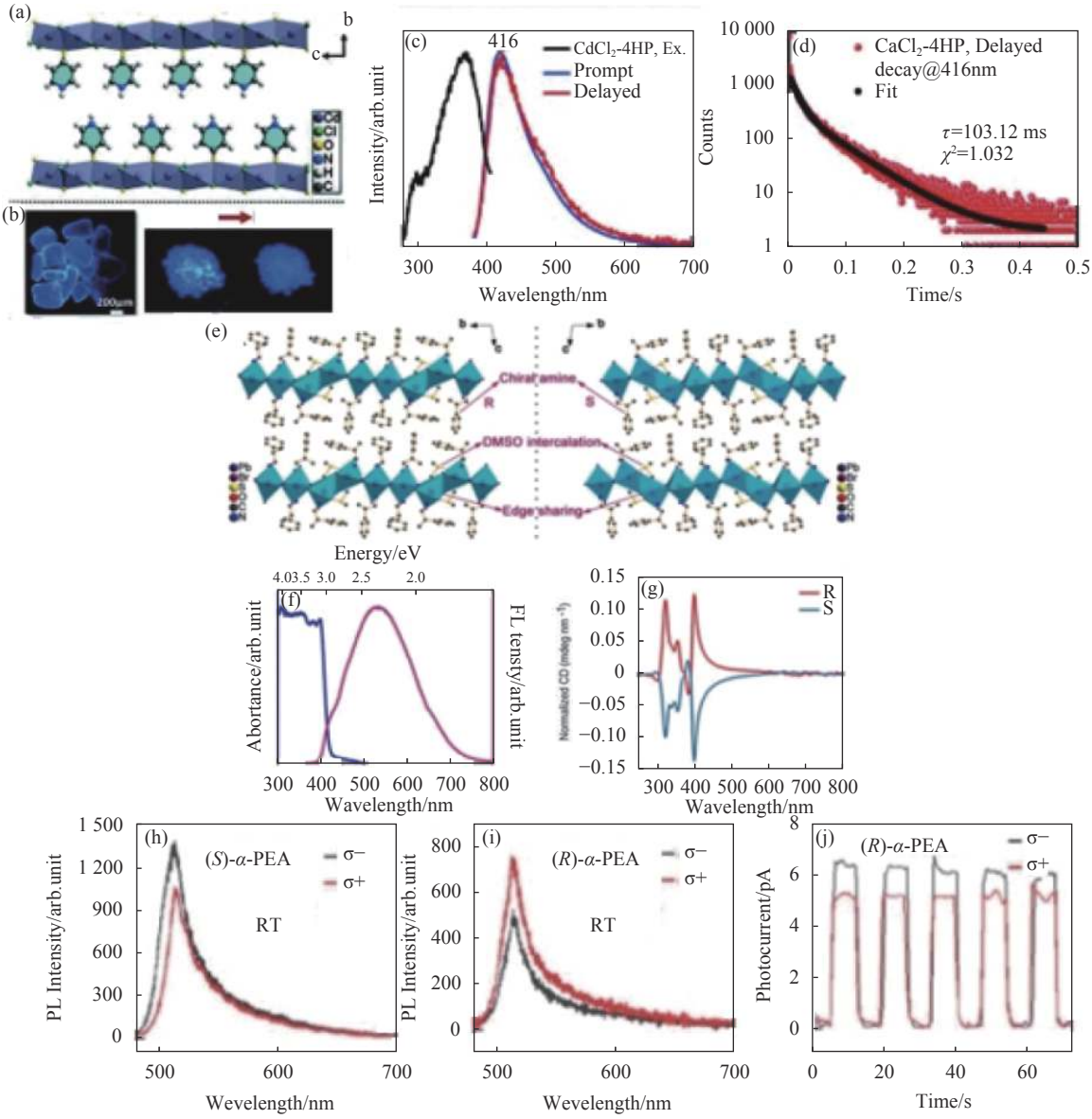

图 7 (a)$CdCl_2$-4HP 晶体的晶体结构; (b) 荧光显微镜图像; (c) 在室温下在 365 nm 处激发的 $CdCl_2$-4HP 的即时 (蓝线) 和延迟 (红线) PL 光谱; (d) $CdCl_2$-4HP 在室温下的时间分辨 PL 衰减曲线 (416 nm), 具有 103.12 ms 的长寿命[37]; (e) 从单晶 XRD 测量获得的手性钙钛矿的晶体结构, 显示出手性, DMSO 嵌入和部分边缘共享的特征; (f) 所制备的 $(R\text{-MPEA})_{1.5}PbBr_{3.5}(DMSO)_{0.5}$ 纳米线的归一化 DRS (漫反射光谱) 和荧光光谱。激发波长: 400 nm; (g) 从 *R*-和 *S*-$(MPEA)_{1.5}PbBr_{3.5}(DMSO)_{0.5}$ 钙钛矿晶体的 DMF 溶液旋涂的薄膜的 CD 光谱[148]; (h),(i)(*S*)-*α*-$(PEA)_2PbI_4$ 和 (*R*)-*α*-$(PEA)_2PbI_4$ 晶体的圆极化 PL 发射; (j)(*R*)-*α*-$(PEA)_2PbI_4$ 器件在偏压为−3 V 的 520 nm 单色 *σ*−和 *σ*+照明下的光学开关特性[149]

Fig.7 (a) Crystal structure ; (b) Fluorescence microscopy images of the $CdCl_2$-4HP crystals; (c) Prompt (blue line) and delayed (red line) PL spectra of $CdCl_2$-4HP excited under 365 nm at room temperature; (d) Time-resolved PL decay profiles (416 nm) of $CdCl_2$-4HP at room temperature with a long lifetime of 103.12 ms[37]; (e) Crystallographic structure of the chiral perovskites as obtained from single crystal XRD measurements, showing the features of chirality, DMSO intercalation, and partial edge sharing; (f) Normalized DRS (diffusive reflectance spectrum) and fluorescence spectra of the as-prepared $(R\text{-MPEA})_{1.5}PbBr_{3.5}(DMSO)_{0.5}$ nanowires. Excitation wavelength: 400 nm; (g) Normalized CD spectra of the films spin-coated from DMF solutions of the *R*- and *S*-$(MPEA)_{1.5}PbBr_{3.5}(DMSO)_{0.5}$ perovskite crystals. Average film thickness for both *R*- and *S*-$(MPEA)_{1.5}PbBr_{3.5}(DMSO)_{0.5}$ is ~ 350 nm[148]; (h), (I) Circularly polarized PL emission of (*S*)-*α*-$(PEA)_2PbI_4$ and (*R*)-*α*-$(PEA)_2PbI_4$ crystals. (J) Optical switching characteristic of the (*R*)-*α*-$(PEA)_2PbI_4$ device under a 520 nm monochromatic σ^- and σ^+ illumination at a bias of −3 V[149]

多材料 (Bi QDs[150], Te 纳米片[151], Se 纳米片[152], 硫化锡[153] 和 BP[154]) 一样在光探测中展现出优异的性质。杂化钙钛矿具有高密度态的直接间隙, 可以增强光与物质之间的相互作用[155]。它们通常具有较大的灵敏度[156], 较高的开/关电流比[157] 和超低暗电流[158]。例如, Tan 等人制备了二维钙钛矿 $(C_4H_9NH_3)_2PbBr_4$ 晶体, 并应用于光探器件[159]。用石墨烯薄膜覆盖后, 该检测器表现出比其他典型二维材料更高的响应度 (2 100 A/W)。类似地, Qian 等人报道了 Sn 基二维钙钛矿 $(PEA)_2SnI_{4-x}Br_x$ (x = 1, 2, 3) 的微米片, 观察到了在 470 nm 的光照下 $(PEA)_2SnI_4$ 的最大光响应度为 3 290 A/W, 检测率为 2.06×10^{11} J[160]。尽管杂化二维钙钛矿在响应度和探测性方面具有优越性, 但它们的有效光谱范围通常比 Bi QDs、Se 纳米片、SnS 等二维材料窄。

2.2 二维钙钛矿的非线性光学

经典的和新兴的二维材料 (例如石墨烯, BP[161], SnS[162], 和 Se 纳米片[163]) 均已应用于非线性光学。例如, 石墨烯具有宽带和强度依赖的非线性光学吸收[164], 以及由活性磷原子组成的单元素二维各向异性材料黑磷[161, 165] 从可见光到[18, 166] 中红外均表现出良好的宽带三阶非线性光学效应 (四波混频和三次谐波产生等) 以及与尺寸相关的非线性光学现象[65]。此外, 黑磷的非中心对称晶格结构[167] 使它可以直接用于二阶非线性光学。SnS 层状材料具有出色的化学和热稳定性[168] 以及可调节的带隙和奇偶量子限制[169], 具有优异的三阶非线性光学响应, 少层的 SnS 被用于全光谱信息转换, 全光开关[162] 和 SA[170]。此外, 理论研究表明, 单层 SnS 独特的非中心对称 C_{2v} (mm2) 点群使其具有 SHG 敏感性[171]。三方晶系的二维 Se 纳米片显示出了良好的非线性光学性质, 这可归因于其大的表面积和与尺寸相关的带隙[163], 其在饱和吸收体与超快光子学方面表现出了大的潜力。

与上述二维材料相比, 二维杂化钙钛矿丰富的化学多样性和结构多样性赋予它们在非线性光学应用的多项优势[53]。其产生的多重量子阱 (MQW) 结构将增强非线性光学特性[172]。此外, 这些层状二维杂化钙钛矿材料的晶格结构和形貌特征十分丰富, 可通过不同的途径调整。与其他经典二维材料制造的低产率、[173] 低质量[174] 和严格的制备条件[175−176] 相比, 通过溶液或气相途径可以轻松地获得高质量且均匀的二维钙钛矿晶体。此外, 有机阳离子在二维杂化钙钛矿中的易取代性为非线性光学的调节提供了便利条件。这些优势推动了二维杂化钙钛矿非线性光学的发展。

2.2.1 二维钙钛矿的二阶非线性光学响应

1961 年, Franken 等人[177] 首次从石英晶体中观察到了 SHG 现象, 这一特殊的现象拉开了非线性光学研究的序幕。之后, 随着新型非线性光学材料的快速发展, 更多的非线性光学效应逐渐被人们所发现。直到现在, SHG 仍是重要的非线性光学现象[178−180]。然而, 由于电偶极子近似推导的二阶非线性光学极化率在中心对称结构中几乎为零, 二阶非线性光学效应在中心对称晶体中是禁阻的[181−182]。因此, 二阶非线性光学只能存在于非中心对称的体系中[183−184]。

大多数二维钙钛矿由于空间结构对称性不具有二阶非线性光学活性。Wang 等人提出了一种发白光的二维杂化钙钛矿 $(2meptH_2)PbBr_4$ (2mept 表示 2-甲基-1, 5-二氨基戊烷)[185]。除了发射范围宽和 PLQY 高以外, 在 1 064 nm 激光 (Nd: YAG) 激发下它还表现出 SHG 响应 (表 1)。单晶 X 射线衍射分析表明该钙钛矿属于极性 Cc(No. 9) 空间群, 该空间群由连续的无机八面体相互挤压产生, 有助于得到显著的偶极矩 ($0.335\,4\times10^{-29}$ C m^{-1})。

铁电性作为材料中的重要特性, 与非对称性密不可分, 因而铁电性也通常伴随二阶非线性光学[186−187]。值得注意的是, 有机阳离子的高度自由运动为铁电性的产生提供了更多的机会[188]。Luo 等人将脂肪族胺合金化, 利用经典的三维无机钙钛矿 $CsPbBr_3$ 合成, 破坏了初级晶体的对称性[189], 生成的 $(C_4H_9NH_3)_2CsPb_2Br_7$ 具有显著的铁电性 (约 4.2μC/cm^{-2}) 和高于 $BaTiO_3$ 的居里温度 (T_c = 412 K)。从室温到 T_c, 随着另一钙钛矿相 (图 8 (b), (c), (d) 和 (e)) 中不对称元素的减少, 它表现出与温度相关的 SHG 响应 (图 8(a))。实际上, SHG 检测是识别不对称性或不对称和对称性之间特殊相位转换的有效且灵敏的途径[190]。

Sun 等人[191] 设计了一种高度偏振敏感的二维杂化钙钛矿铁电体 $[CH_3(CH_2)_3NH_3]_2(CH_3NH_3)Pb_2Br_7$, 并

表 1 二维钙钛矿的非线性光学

Tab.1 2D perovskites for NLO

Chemical formula	Metal	Halogen	Organic ligand	Phase	NLO property	Reference
$(2meptH_2)PbBr_4$	Pb	Br	2-methyl-1,5-diaminopentane	R-P	SHG	185
$(C_4H_9NH_3)_2CsPb_2Br_7$	Pb	Br	$C_4H_9NH_3$	R-P	SHG	189
$[CH_3(CH_2)_3NH_3]_2(CH_3NH_3)Pb_2Br_7$	Pb	Br	$CH_3(CH_2)_3NH_3$, CH_3NH_3	R-P	SHG	191
$(BA)_2(EA)_2Pb_3I_{10}$	Pb	I	*n*-butylammonium, ethylammonium	R-P	SHG	192
$[(C_6H_5CH_2NH_3)_2]PbCl_4$	Pb	Cl	$C_6H_5CH_2NH_3$	R-P	SHG	199
R/*S*-$(MPEA)_{1.5}PbBr_{3.5}(DMSO)_{0.5}$	Pb	Br	methylphenethylamine	-	SHG	148
[*R*/*S*-LIPF]$_2PbI_4$	Pb	I	*R*/*S*-1-(4-chlorophenyl)ethylammonium	R-P	SHG	200
$(C_6H_5C_2H_4NH_3)_2PbI_4$	Pb	I	$C_6H_5C_2H_4NH_3$	R-P	THz	203
$(CH_3(CH_2)_3NH_3)_2(CH_3NH_3)_{n-1}Pb_nI_{3n+1}$	Pb	I	$CH_3(CH_2)_3NH_3$, CH_3NH_3	R-P	THG	207
$(C_4H_9NH_3)_2PbBr_4$	Pb	Br	$C_4H_9NH_3$	R-P	THG	209
$(C_4H_9NH_3)_2PbI_4$	Pb	I	$C_4H_9NH_3$	R-P	THG	209
$(C_4H_9NH_3)_2(CH_3NH_3)Pb_2I_7$	Pb	I	$C_4H_9NH_3$, CH_3NH_3	R-P	THG	209
$(C_4H_9NH_3)_2(CH_3NH_3)_2Pb_3I_{10}$	Pb	I	$C_4H_9NH_3$, CH_3NH_3	R-P	THG	209
$(C_4H_9NH_3)_2(NH_2CHNH_2)Pb_2Br_7$	Pb	Br	$C_4H_9NH_3$, NH_2CHNH_2	R-P	2PA	213
$(PEA)_2PbI_4$	Pb	I	phenethylamine	R-P	2PA	214
$(BA)_2PbI_4/(BA)_2MAPb_2I_7)$	Pb	I	*n*-$C_4H_9NH_3$	R-P	2PA	215
$(PEA)_2(MA)_4Pb_5Br_{16}$	Pb	Br	phenethylamine, methylammonium	R-P	2PL	217
$(C_4H_9NH_3)_2PbBr_4$	Pb	Br	$C_4H_9NH_3$	R-P	3PA	226
$(OA)_2PbBr_4$	Pb	Br	octyl ammonium	R-P	5PA	227
$(C_6H_5C_2H_4NH_3)_2PbI_4$	Pb	I	$C_6H_5C_2H_4NH_3$	R-P	SA	234
$(BA)_2(MA)_{n-1}Pb_nBr_{3n+1}$	Pb	Br	*n*-$C_4H_9NH_3$, methylammonium	R-P	SA	235

用于检测短波偏振光[191]。*P-E* 磁滞回线记录表明，在 318 K 时它具有 3.6 μC/cm^2 的超强自发极化 (P_s)，可检测到的 SHG 响应显示出在室温下稳定的 SHG 强度约为 0.4×KDP。该钙钛矿铁电体还显示出较强的二色性比 (I^c_{ph}/I^a_{ph}≈2.0)，同时具有出色的灵敏检测率 (约 10^9Jones) 和短波区域的灵敏响应率 (约 20 μs)。该课题组还研究了在高温下反铁电二维多层杂化钙钛矿 ($(BA)_2(EA)_2Pb_3I_{10}$ (BA =正丁基铵，EA =乙基铵)[192]。高度依赖温度的 SHG 活性证实了该钙钛矿中存在非中心对称结构。*P-E* 磁滞回线验证了铁电和反铁电的存在，该性质伴有 P_s 为 5.6 μC/cm^2 (室温) 的双轴铁电和高居里点 (约 363 K)。同时，出色的储能效率 (65%-83%) 赋予了其高效的储电潜力。此外，压电材料也与材料的非中心对称性和非线性光学密切相关[193−195]。然而，大多数二维钙钛矿压电材料是全无机的。例如，$CsLaNb_2O_7$[196]、$RbBi_2Ti_2NbO_{10}$[197]、$CsBi_2Ti_2TaO_{10}$[197] 和 Li*R*TiO_4[198](*R* 代表稀土元素) 压电材料均具有清晰的 SHG 信号，表现出特征的不对称性。

因为层数可灵活变化且能替换各种阳离子，二维钙钛矿往往比其他二维层状材料更容易进行构造的调整。因此，常见 SHG 响应随钙钛矿极化的改变而变化。最近，Wei 等人使用 SHG 检测方法，观察了具有极性空间基团 ($Cmc2_1$) 的二维杂化钙钛矿 $[(C_6H_5CH_2NH_3)_2]PbCl_4$ 纳米片中的范德华 (vdW) 相互作用[199]。如图 9(a) 和图 9(b) 所示，沿晶体 *b* 轴和 *c* 轴极化的 SHG 效应以及 SHG 强度的各向异性表明，由于 vdW 相互作用的微小变化，随着纳米片厚度的减小，信号强度有所衰减。

如前所述，手性官能团的引入可以诱导二维钙钛矿形成非中心对称空间构型，促进二阶非线性光学效应的产生与应用。例如，二维手性钙钛矿纳米线 *R*-$(MPEA)_{1.5}PbBr_{3.5}(DMSO)_{0.5}$ 显示出在多种波长的激光下泵浦的突出 SHG 信号 (图 10(a))。它具有较高的二阶 NLO 系数 (d_{eff} 约 0.68 pm / V)，激光损伤阈值为 8.6×10^4 W/cm^2。进一步的偏振依赖的 SHG 测量 (图 10(c)) 结果表明，手性钙钛矿在线性偏振激光下 (图 10(b))

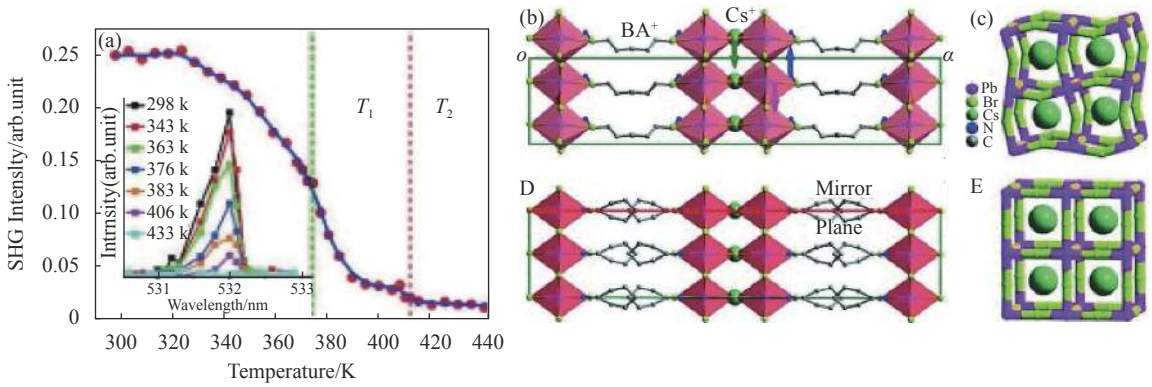

图 8 (a)$(C_4H_9NH_3)_2CsPb_2Br_7$ 的温度依赖性 SHG 信号。插图表示 $(C_4H_9NH_3)_2CsPb_2Br_7$ 在不同温度下的晶体结构。在 293 K: (b) 沿结晶 *b* 轴观察, (c) 钙钛矿骨架。箭头表示沿 *c* 轴的相对位移;在 420 K: (d) 高度对称的结构堆积和 (e) 钙钛矿骨架[189]

Fig.8 (A) Temperature dependent SHG signals of $(C_4H_9NH_3)_2CsPb_2Br_7$. Inset: Crystal structures of $(C_4H_9NH_3)_2CsPb_2Br_7$ at different temperatures. At 293 K: (b) viewed along the crystallographic *b*-axis and (c) the perovskite framework. The arrows indicate the relative displacements along the crystallographic *c*-axis. At 420 K: (d) highly symmetric structure packing and (E) perovskite framework[189]

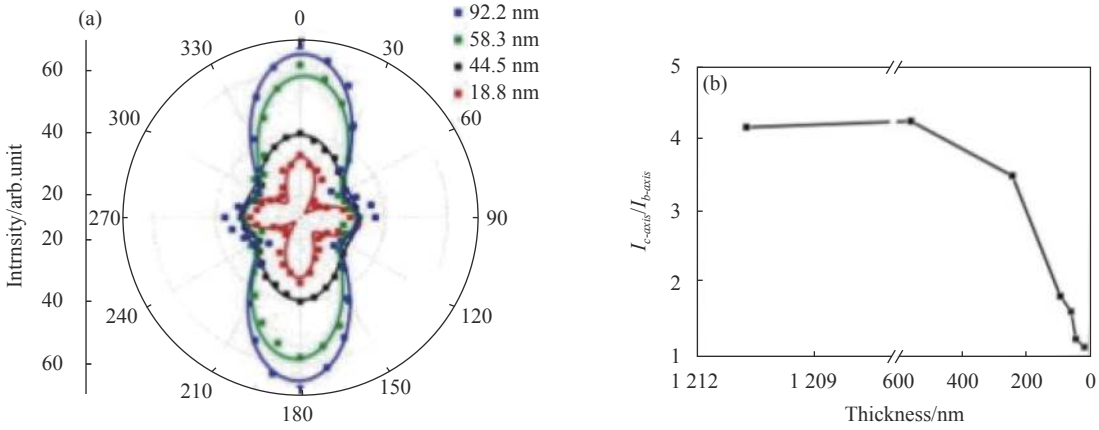

图 9 (a) 二维 $[(C_6H_5CH_2NH_3)_2]$ 钙钛矿纳米片的极性 SHG 强度图; (b)SHG 强度各向异性 ($I_{c\text{-axis}}/I_{b\text{-axis}}$) 取决于所测量的纳米片的厚度[199]

Fig.9 (a) Polar SHG intensity plots of the 2D $[(C_6H_5CH_2NH_3)_2]PbCl_4$ perovskite nanosheets. (b) SHG intensity anisotropy ($I_{c\text{-axis}}/I_{b\text{-axis}}$) dependent on the thickness of the measured nanosheets[199]

显示出高达 96.4% 的大偏振比, 在圆偏振光泵浦下 (图 10(d)) 也显示出清晰的非线性光学圆二色性。

之后不久, Xiong 等人[200] 将手性阳离子对映体 (*R*/*S*-LIPF, LIPF = 1-(4-氯苯基) 乙铵) 与二维碘化铅钙钛矿结合, 得到同时具有铁电和 SHG 响应的二维钙钛矿材料[200]。这对对映体是通过简单的分子调制在室温下极性 *P*1 空间群中结晶的, 这表明了自发极化的存在 (计算值约为 13.96 μC/ cm^{-2})。*R*-LIPF($T_c(R)$ = 483.0 K) 和 *S*-LIPF($T_c(S)$ = 473.2 K) 钙钛矿的相变温度 T_c 明显不同, 这与一般对映异构体不同。从 SHG 光谱来看, *R*/*S*-LIPF 显示出适中的 SHG 强度 (大约是 KDP 参考的一半), 当温度上升, 接近 T_c 时强度逐渐衰减。压电响应力显微镜 (PFM) 的磁滞回线显示了 *R*-LIPF 薄膜具有相当大的局部矫顽电压响应 (≈112 V), 这解释了其显著的铁电性能和可转换的极化效应。

由二阶非线性光学材料产生的太赫兹 (THz) 辐射 (集中在 0.1~10 THz 频率范围内)[201−202], 已经迅速发展并应用于通信、检测和传感设施。但是在实际应用上, 很少通过二维钙钛矿生成和调制 THz 辐射。2017 年, Chanana 等人[203] 通过沉积在半导体衬底上的二维杂化钙钛矿 $(C_6H_5C_2H_4NH_3)_2PbI_4$ (PEPI) 完成了 THz 辐射的选择性调制[203], 可以通过改变层数灵活地调节多层钙钛矿的带隙和激子吸收带。与纯硅

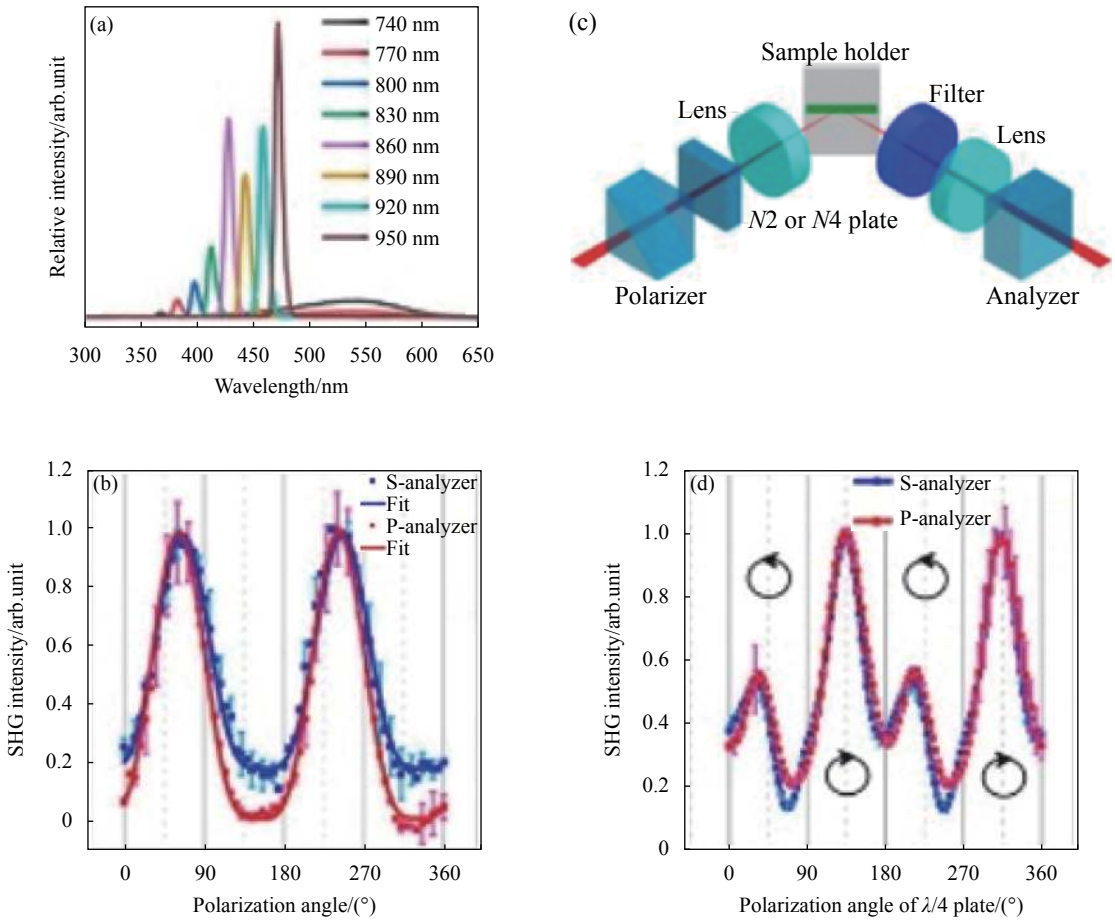

图 10 (a) 以各种波长泵浦的 $(R\text{-MPEA})_{1.5}PbBr_{3.5}(DMSO)_{0.5}$ 纳米线的归一化 NLO 光谱; (b) 来自水平取向的 $((R\text{-MPEA})_{1.5}PbBr_{3.5}(DMSO)_{0.5}$ 纳米线的 SHG 强度与由 $\lambda/2$ 波片调谐的线性极化角的关系; (c) NLO 测试示意图; (d) 纳米线的 SHG 强度是 $\lambda/4$ 波片旋转角的函数。如箭头所示, 当旋转角为 45°和 225°时, 泵为左旋圆极化, 当旋转角为 135°和 315°时, 泵为右旋圆极化[148]。

Fig.10 (a) Normalized NLO spectra of a $(R\text{-MPEA})_{1.5}PbBr_{3.5}(DMSO)_{0.5}$ nanowire pumped at various wavelengths; (b) SHG intensity from a horizontally oriented $(R\text{-MPEA})_{1.5}PbBr_{3.5}(DMSO)_{0.5}$ nanowire as function of the linear polarization angle as tuned by the $\lambda/2$ plate; (c) Schematics of the NLO measurements; (d) SHG intensity from the nanowire as function of the rotation angle of the $\lambda/4$ plate. The pump was left-handed circularly polarized when the rotation angle was 45° and 225°, and was right-handed circularly polarized when the rotation angle was 135° and 315°, as indicated by the arrows [148]

半导体相比, 钙钛矿/硅晶片上的宽带太赫兹吸收明显优越[204]。

2.2.2 二维钙钛矿的三阶及高阶非线性光学

三阶非线性光学不受非中心对称结构的限制, 因此, 更多的二维材料可以用于三阶非线性光学[205−206]。Saouma 等人通过三次谐波产生 (THG), 探索了二维 R-P 钙钛矿 $(CH_3(CH_2)_3NH_3)_2(CH_3NH_3)_{n-1}Pb_nI_{3n+1}$ (n = 1−4) 的三阶非线性光学[207]。就整个红外 (IR) 的 THG 系数而言, 它的表现优于其三维对应物 $MAPbBr_3$ 和参考材料 $AgGaSe_2$, $\chi^{(3)}$ 范围为 $(2.6 \pm 0.5)\times 10^{-11}$ esu 到 $(5.6 \pm 1.0)\times 10^{-11}$ esu。随着钙钛矿尺寸的减小, 激光诱导的损伤阈值也得到了改善。此外, 这些二维钙钛矿都具有对光学损伤的高弹性。一般认为二维 R-P 钙钛矿中的单量子阱结构有利于增强三阶非线性光学[208]。Abdelwahab 等人从四个二维 R-P 钙钛矿 $(C_4H_9NH_3)_2PbBr_4(Br_{n=1})$,$(C_4H_9NH_3)_2PbI_4$ ($I_{n=1}$), $(C_4H_9NH_3)_2(CH_3NH_3)Pb_2I_7(I_{n=2})$ 和 $(C_4H_9NH_3)_2(CH_3NH_3)_2Pb_3I_{10}$ ($I_{n=3}$) 的单晶中机械剥离纳米薄片[209]。这些二维 R-P 钙钛矿纳米片几乎在整个可见光范围内都能产生强 THG 信号。$(C_4H_9NH_3)_2(CH_3NH_3)Pb_2I_7$ R-Ps 的三阶非线性光学极化率 $\chi^{(3)}$ 为 1.12×10^{-17} m^2 V^{-2}, 远高于常规二维材料[210]。

双光子吸收 (2PA) 也是重要的三阶非线性光学效应, 其强度和深度呈二次关系[211]。该现象有望提高太阳能电池的光捕获能力[206] 和光探测器的灵敏度[212]。Luo 等人报道了具有突出双光子吸收效应的铁电杂化钙钛矿 $(C_4H_9NH_3)_2(NH_2CHNH_2)Pb_2Br_7$ 单晶[213]。在 $[Pb_2Br_7]_\infty$八面体中, 独特的双层堆叠紧紧限制了载流子移动。通过 Z 扫描技术测定了其双光子吸收系数为 5.76×10^3 cm GW^{-1}, 高于传统的全无机钙钛矿。DSC 曲线揭示了可逆的 (322 K/318 K) 铁电相变, 并显示了 3.8 μC/cm^{-2} 的自发极化。为了增强 2PA 的光致发光, Lu 等人设计了一种由 SiO_2 微球组成的复合结构, 并将其转移到均匀的二维钙钛矿片中[214]。通过使用透明胶带, 从制备的 $(PEA)_2PbI_4$ 钙钛矿薄膜中机械剥落这些二维钙钛矿片, 然后覆盖上均匀分散的介电微球。二维钙钛矿薄片中的混合电介质结构不仅使泵浦激光集中, 而且抑制了非辐射损耗。在微球的协同作用下, 2PA 诱导的光致发光发射比初始提高了两个数量级 (图 11)。除了均质钙钛矿晶体以外, 二维钙钛矿中的异质结构也有望展现出优异的非线性光学性能。Wang 等人探索了 $(BA)_2PbI_4$/$(BA)_2MAPb_2I_7$) (BA = n−$C_4H_9NH_3$) 异质结构的非线性光学特性[215]。将 800~1 200 nm 的多光子诱导光致发光 (MPL) 与非线性透射率测量相结合, 可以测定二维钙钛矿异质结构比纯 $(BA)_2PbI_4$ (4.56 cm MW^{-1}) 和 $(BA)_2MAPb_2I_7$ (6.25 cm MW^{-1}) 具有更大的 2PA 系数 (44 cm MW^{-1})。另外, 设计的异质结构在红外波段中有 10^{-7} A W^{-1} 的高响应度。该材料优异的非线性光学特性可能是源于钙钛矿异质结构中通过天线效应 (antenna-like effect) 进行的非辐射能量转移。除了双光子吸收外, 双光子发光 (2PL) 也是在生物成像等实际应用中有价值的非线性光学效应[216]。Zhu 等人[217] 通过巧妙的反溶剂处理方法合成了一种准二维钙钛矿 $(PEA)_2(MA)_4Pb_5Br_{16}$ (n = 5)[217]。在 980 nm 的连续波 (CW) 激发下, 直接通过光学激发间隙态可以观察到双光子上转换发光。但是, 当 n 小于 5 时, 2PL 响应变得不再明显。

为了增强多光子吸收 (MPA) 截面 ($\eta\times\sigma_n$, η 和 σ_n 分别代表光致发光量子产率和截面), 更高阶的非线性光学效应, 例如三光子吸收 (3PA)[218], 四光子吸收 (4PA)[219], 甚至五光子吸收 (5PA)[220] 也相继出现[221−222]。对于高分辨率成像、光限幅、泵浦激射等方面的应用, 多光子荧光需要更大的穿透深度、更小的背景荧光和更低的光损伤[223−225]。最近, Ji 等人比较了多层钙钛矿 $(C_4H_9NH_3)_2PbBr_4$ 与三维钙钛矿 3PA 系数的差异[226]。根据二维激子量子微扰模型, 在约 1 000 nm 的激光激发下, 3PA 系数应为 2~7 cm^3 GW^{-2}。三光子激发光致发光 (3PL) 与理论推测非常吻合, 证实了二维激子在增强 3PA 系数中的关键作用。此外, 该理论还推论出, 由于最终激子态的线宽低 (< 1 meV), 低温会将 3PA 系数提高至少 2 个数量级。

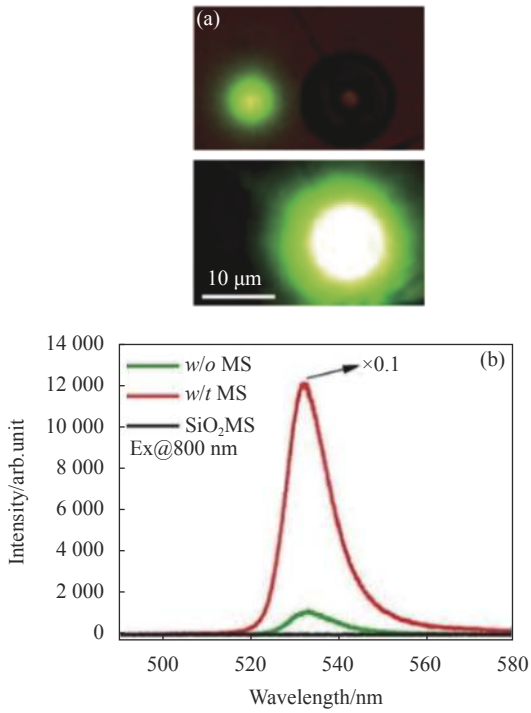

图 11 (a) 在 0.1 mW 的激发功率下, 不带 (上图) 和带 (下图)SiO_2 微球的钙钛矿片的 2PL 图像; (b) 钙钛矿裸片 (不带 MS, 绿色曲线) 和钙钛矿-微球混合介电结构 (不带 MS, 红色曲线) 的 2PL 光谱。SiO_2 微球在该波段内没有发射 (黑色曲线)[214]

Fig.11 (a) 2PL images of the perovskite flake without (top panel) and with (bottom panel) SiO_2 microsphere under an excitation power of 0.1 mW, respectively; (b) 2PL spectra for a bare perovskite flake (*w/o* MS, green curve) and a perovskite-microsphere hybrid dielectric structure (*w/t* MS, red curve). The SiO_2 microsphere shows no emission within this waveband (black curve)[214]

传统的半导体材料或有机晶体通常很难达到高的 4PA 或 5PA 非线性光学截面。Chen 等人[227] 提出了一种自制的核-壳卤化物钙钛矿胶体纳米晶体, 该晶体包含三维 $MAPbBr_3$ 核和 $(OA)_2PbBr_4$ 壳 (OA = 辛

基胺), 具有超高的 5PA 系数[227]。包裹在核上的 $(OA)_2PbBr_4$ 壳层为 $MAPbBr_3$ 提供了更强的量子限域作用, 并实现了表面钝化, 与裸露的 $MAPbBr_3$ 纳米晶体相比, σ_5 和荧光量子产率都得到了提升[228−230]。使用波长为 800 nm 的 Z 扫描测量[231] 研究该核-壳多维钙钛矿, 其 $\eta\sigma_n$ 约为 10^{-136} cm^{10} s^4 $photon^{-4}$, 比报道的有机染料高出 9 个数量级[231]。

二维钙钛矿优异的非线性光学特性和光学稳定性已将其应用扩展到超快激光光学。激光发射源自饱和吸收 (SA), 饱和吸收体可以选择性滤出低强度光[232]。与三维钙钛矿纳米片产生脉冲不同[233], Hong 等人制备了二维杂化钙钛矿 $(C_6H_5C_2H_4NH_3)_2PbI_4$(缩写为 PEPI) 微晶薄膜, 用于光纤激光器的超快锁模[234]。基于 PEPI 饱和吸收体的作用, 在异常情况下, 孤子脉冲 (381 fs) 覆盖了 C 和 L 波段, 在正常色散状态下, 耗散孤子脉冲在 1561.2 nm 的中心形成, 稳定脉冲持续时间为 3.4 ps, 具有可靠的重复性。此外, 可以通过在 C 波段和 L 波段改变光增益调节激光波长。Fu 等人在密闭溶液中通过 PDMS(聚二甲基硅氧烷) 模板途径, 以二维钙钛矿 $(BA)_2(MA)_{n-1}Pb_nBr_{3n+1}$ 为基础设计了大面积微环激光器阵列[235]。在放大自发发射 (ASE) 过程中, 发现 $n = 6$ 微环具有 112 cm^{-1} 的较高增益系数 (G), 并且具有 13.6 μJ cm^{-2} 的低阈值通量, 其性能要比以前报道的三维钙钛矿类似物[236−237] 高出许多。在回音壁模式下, 均匀的薄膜谐振腔获得了约 2600 的品质因子。

3 结论和展望

作为一种高性能的半导体材料, 低成本和简单的制造工艺已经使二维有机-无机杂化钙钛矿具备了诸如石墨烯、TMD 和 BP 等传统的二维半导体材料的优势。同时, 有机阳离子的种类比无机阳离子丰富, 这些有机阳离子的多样性使得二维杂化钙钛矿在调节层间距离和结构变形方面具有很高的自由度和灵活性。独特的自然形成的多量子阱效应导致其具有巨大的激子结合能和更高的稳定性, 而层数 n 在调节钙钛矿的带隙中起着至关重要的作用, 使其成为了光子学和光电子学应用的热点。此外, 手性有机官能团的引入突破了传统杂化钙钛矿中的空间对称性限制, 扩展了二维钙钛矿在二阶非线性应用中的新途径。尽管如此, 该领域的研究和技术仍处于起步阶段。例如, THz 的产生、检测和调制、光合频产生 (SFG)、光差频产生 (SFG) 和 Kerr 效应的研究仍值得进一步探索。还值得一提的是, 等离子体纳米结构具有非凡的光学特性, 可以通过等离激元激发来增强二维杂化钙钛矿中的光-质相互作用[238]。通过掺入等离子体金属纳米粒子, 钙钛矿-等离子体半导体中光学和光电性能将显著提高[239−240]。等离子体效应带来的增强非线性特性已经扩展到非线性等离子体研究的新领域。在具有简单的等离子体纳米粒子的二维钙钛矿中, 也已经观察到 SHG、THG、多光子吸收或发射等的增强。此外, 等离激元效应显示出了其在设计制作低功率、小尺寸和快速响应的光学设备方面的巨大潜力[241]。

但是, 二维钙钛矿领域也存在一些不容忽视的短板, 包括在热、光和湿度等刺激下的不稳定性, 以及源自重金属的毒性问题。尽管插入有机阳离子可以增强二维钙钛矿的抗性和适应性, 但它本质上不能解决这些问题。与其他二维材料不同, 即使它们的非线性光学性质十分适合生物成像和生物传感[242−244], 但本身高含量的重金属和卤元素阻碍了它们在生物医学领域的应用。为了减轻含铅钙钛矿毒性的影响, 一些关于无铅杂化钙钛矿的研究大量涌现。但是, 这些二维无铅杂化钙钛矿的非线性光学研究仍处于起步阶段。因此, 二维钙钛矿中的不稳定性和毒性是阻碍研究和工业发展的主要因素。此外, 二维钙钛矿异质结构的出现也为改善性能提供了一种新方法。BP、TMDs、石墨烯等的材料的加入可形成电荷载流子传输和光电门效应的可调屏障, 以优化原始钙钛矿材料的性能 (例如光电探测器或光电晶体管的灵敏度) 并激发其纳米光子功能。高质量、长期稳定、环境友好、效率更高的二维有机-无机杂化钙钛矿将为光子学、电光、光电和其他重要的跨学科领域中综合化应用开辟新的道路。

参考文献:

[1] Novoselov K S, Geim A K, Morozov S V, et al. Electric field effect in atomically thin carbon films [J]. ***Science***, 2004, 306: 666-669.

[2] You J W, Bongu S R, Bao Q, et al. Nonlinear optical properties

and applications of 2D materials: theoretical and experimental aspects [J]. ***Nanophotonics***, 2018, 8: 63-97.

[3] Yun Q, Li L, Hu Z, et al. Layered transition metal dichalcogenide-based nanomaterials for electrochemical energy storage [J]. ***Adv Mater***, 2019, 32: 1903826.

[4] Hu F, Fei Z. Recent progress on exciton polaritons in layered transition-metal dichalcogenides [J]. ***Adv Opt Mater***, 2019: 1901003.

[5] Cho K, Pak J, Chung S, et al. Recent advances in interface engineering of transition-metal dichalcogenides with organic molecules and polymers [J]. ***ACS Nano***, 2019, 13: 9713-9734.

[6] Li G, Li Y, Liu H, et al. Architecture of graphdiyne nanoscale films [J]. ***Chem Commun***, 2010, 46: 3256-3258.

[7] Li Y, Xu L, Liu H, et al. Graphdiyne and graphyne: from theoretical predictions to practical construction [J]. ***Chem Soc Rev***, 2014, 43: 2572-2586.

[8] Jia Z, Li Y, Zuo Z, et al. Synthesis and properties of 2D carbon—graphdiyne [J]. ***Acc Chem Res***, 2017, 50: 2470-2478.

[9] Wu L, Dong Y, Zhao J, et al. Kerr nonlinearity in 2D graphdiyne for passive photonic diodes [J]. ***Adv Mater***, 2019, 31: 1807981.

[10] Dong Y, Zhao Y, Chen Y, et al. Graphdiyne-hybridized n-doped TiO_2 nanosheets for enhanced visible light photo-catalytic activity [J]. ***J Mater Sci***, 2018, 53: 8921-8932.

[11] Xue Z, Zhu M, Dong Y, et al. An integrated targeting drug delivery system based on the hybridization of graphdiyne and MOFs for visualized cancer therapy [J]. ***Nanoscale***, 2019, 11: 11709-11718.

[12] Chakraborty C, Vamivakas N, Englund D. Advances in quantum light emission from 2D materials [J]. ***Nanophotonics***, 2019, 8: 2017-2032.

[13] Caldwell J D, Aharonovich I, Cassabois G, et al. Photonics with hexagonal boron nitride [J]. ***Nat Rev Mater***, 2019, 4: 552-567.

[14] Kanahashi K, Pu J, Takenobu T. 2D materials for large-area flexible thermoelectric devices [J]. ***Adv Energy Mater***, 2019: 1902842.

[15] Khan K, Tareen A K, Aslam M, et al. Recent advances in two-dimensional materials and their nanocomposites in sustainable energy conversion applications [J]. ***Nanoscale***, 2019, 11: 21622-21678.

[16] Sun J, Choi Y, Choi Y J, et al. 2D –organic hybrid heterostructures for optoelectronic applications [J]. ***Adv Mater***, 2019, 31: 1803831.

[17] Lu S, Zhao C, Zou Y, et al. Third order nonlinear optical property of Bi_2Se_3 [J]. ***Opt Express***, 2013, 21: 2072-2082.

[18] Guo Z, Zhang H, Lu S, et al. From black phosphorus to phosphorene: basic solvent exfoliation, evolution of raman scattering, and applications to ultrafast photonics [J]. ***Adv Funct Mater***, 2015, 25: 6996-7002.

[19] Lu S B, Miao L L, Guo Z N, et al. Broadband nonlinear optical response in multi-layer black phosphorus: an emerging infrared and mid-infrared optical material [J]. ***Opt Express***, 2015, 23: 11183-11194.

[20] Cao R, Wang H D, Guo Z N, et al. Black phosphorous/indium selenide photoconductive detector for visible and near-infrared light with high sensitivity [J]. ***Adv Opt Mater***, 2019, 7: 1900020.

[21] Wang C, Liu H, Bian G, et al. Metal-layer assisted growth of ultralong quasi-2D MOF nanoarrays on arbitrary substrates for accelerated oxygen evolution [J]. ***Small***, 2019, 15: 1906086.

[22] Xue Y, Zhang Q, Wang W, et al. Opening two-dimensional materials for energy conversion and storage: a concept [J]. ***Adv Energy Mater***, 2017, 7: 1602684.

[23] Pang J, Mendes R G, Bachmatiuk A, et al. Applications of 2D MXenes in energy conversion and storage systems [J]. ***Chem Soc Rev***, 2019, 48: 72-133.

[24] Sun Z, Martinez A, Wang F. Optical modulators with 2D layered materials [J]. ***Nat Photonics***, 2016, 10: 227-238.

[25] Wang M, Cai S, Pan C, et al. Robust memristors based on layered two-dimensional materials [J]. ***Nat Electron***, 2018, 1: 130-136.

[26] Dong R, Lan C, Li F, Yip S, et al. Incorporating mixed cations in quasi-2D perovskites for high-performance and flexible photodetectors [J]. ***Nanoscale Horiz***, 2019, 4: 1342-1352.

[27] Anichini C, Czepa W, Pakulski D, et al. Chemical sensing with 2D materials [J]. ***Chem Soc Rev***, 2018, 47: 4860-4908.

[28] Iannaccone G, Bonaccorso F, Colombo L, et al. Quantum engineering of transistors based on 2D materials heterostructures [J]. ***Nat Nanotechnol***, 2018, 13: 183-191.

[29] Novoselov K S, Mishchenko A, Carvalho A, et al. 2D materials and van der Waals heterostructures [J]. ***Science***, 2016, 353: aac9439.

[30] Shiue R J, Efetov Dmitri K, Grosso G, et al. Active 2D materials for on-chip nanophotonics and quantum optics [J]. ***Nanophotonics***, 2017, 6: 1329-1342.

[31] Stoumpos C C, Kanatzidis M G. Halide perovskites: poor man's high-performance semiconductors [J]. ***Adv Mater***, 2016, 28: 5778-5793.

[32] Wang L, Zhou H, Hu J, et al. A Eu^{3+}-Eu^{2+} ion redox shuttle

imparts operational durability to Pb-I perovskite solar cells [J]. ***Science***, 2019, 363: 265-270.

[33] Kostopoulou A, Brintakis K, Nasikas Nektarios K, et al. Perovskite nanocrystals for energy conversion and storage [J]. ***Nanophotonics***, 2019, 8: 1607-1640.

[34] Jeon N J, Na H, Jung E H, et al. A fluorene-terminated hole-transporting material for highly efficient and stable perovskite solar cells [J]. ***Nat Energy***, 2018, 3: 682-689.

[35] Kovalenko M V, Protesescu L, Bodnarchuk M I. Properties and potential optoelectronic applications of lead halide perovskite nanocrystals [J]. ***Science***, 2017, 358: 745-750.

[36] Dou L, Wong A B, Yu Y, et al. Atomically thin two-dimensional organic-inorganic hybrid perovskites [J]. ***Science***, 2015, 349: 1518-1521.

[37] Zhou B, Yan D. Simultaneous long-persistent blue luminescence and high quantum yield within 2D organic-metal halide perovskite micro/nanosheets [J]. ***Angew Chem Int Ed***, 2019, 58: 15128-15135.

[38] Lu S, Ge Y, Sun Z, et al. Ultrafast nonlinear absorption and nonlinear refraction in few-layer oxidized black phosphorus [J]. ***Photon Res***, 2016, 4: 286-292.

[39] Song Y, Chen Y, Jiang X, et al. Nonlinear few-layer MXene-assisted all-optical wavelength conversion at telecommunication band [J]. ***Adv Opt Mater***, 2019, 7: 1801777.

[40] Nayak A, Park J, De Mey K, et al. Large hyperpolarizabilities at telecommunication-relevant wavelengths in donor-acceptor-donor nonlinear optical chromophores [J]. ***ACS Cent Sci***, 2016, 2: 954-966.

[41] Li G, Zhang S, Zentgraf T. Nonlinear photonic metasurfaces [J]. ***Nat Rev Mater***, 2017, 2: 17010.

[42] Ye W, Zeuner F, Li X, et al. Spin and wavelength multiplexed nonlinear metasurface holography [J]. ***Nat Commun***, 2016, 7: 11930.

[43] Xing C, Jing G, Liang X, et al. Graphene oxide/black phosphorus nanoflake aerogels with robust thermo-stability and significantly enhanced photothermal properties in air [J]. ***Nanoscale***, 2017, 9: 8096-8101.

[44] Jiang X, Liu S, Liang W, et al. Broadband nonlinear photonics in few-layer MXene $Ti_3C_2T_x$ (T = F, O, or OH) [J]. ***Laser Photonics Rev***, 2018, 12: 1700229.

[45] Lu L, Tang X, Cao R, et al. Broadband nonlinear optical response in few-layer antimonene and antimonene quantum dots: a promising optical kerr media with enhanced stability [J]. ***Adv Opt Mater***, 2017, 5: 1700301.

[46] Welford W T. The Principles of Nonlinear Optics [J]. ***Journal of Modern Optics***, 1985, 21(4): 400.

[47] Dalton L R, Harper A W, Ghosn R, et al. Synthesis and processing of improved organic second-order nonlinear optical materials for applications in photonics [J]. ***Chem Mater***, 1995, 7: 1060-1081.

[48] Saleh B E A, Teich M C. Fundamentals of photonics~ Wiley [J]. ***Spie Org***, 2007, 45: 87.

[49] Zhang R, Fan J, Zhang X, et al. Nonlinear optical response of organic –onorganic halide perovskites [J]. ***ACS Photonics***, 2016, 3: 371-377.

[50] Xu J, Semin S, Rasing T, et al. Organized chromophoric assemblies for nonlinear optical materials: towards (sub)wavelength scale architectures [J]. ***Small***, 2015, 11: 1113-1129.

[51] Di Bella S. Second-order nonlinear optical properties of transition metal complexes [J]. ***Chem Soc Rev***, 2001, 30: 355-366.

[52] Li X, Semin S, Estrada L A, et al. Strong optical nonlinearities of self-assembled polymorphic microstructures of phenylethynyl functionalized fluorenones [J]. ***Chin Chem Lett***, 2018, 29: 297-300.

[53] Xu J, Li X, Xiong J, et al. Halide perovskites for nonlinear optics [J]. ***Adv Mater***, 2019, 32: 1806736.

[54] Wang A, Ye J, Humphrey M G, et al. Graphene and carbon-nanotube nanohybrids covalently functionalized by porphyrins and phthalocyanines for optoelectronic properties [J]. ***Adv Mater***, 2018, 30: 1705704.

[55] Zhao M, Peng R, Zheng Q, et al. Broadband optical limiting response of a graphene–PbS nanohybrid [J]. ***Nanoscale***, 2015, 7: 9268-9274.

[56] Zheng C, Lei L, Huang J, et al. Facile control of metal nanoparticles from isolated nanoparticles to aggregated clusters on two-dimensional graphene to form optical limiters [J]. ***J Mater Chem C***, 2017, 5: 11579-11589.

[57] Li X. Design of novel graphdiyne-based materials with large second-order nonlinear optical properties [J]. ***J Mater Chem C***, 2018, 6: 7576-7583.

[58] Shehzadi K, Ayub K, Mahmood T. Theoretical study on design of novel superalkalis doped graphdiyne: A new donor–acceptor (D-π-A) strategy for enhancing NLO response [J]. ***Appl Surf Sci***, 2019, 492: 255-263.

[59] Guo J, Shi R, Wang R, et al. Graphdiyne-polymer nanocomposite as a broadband and robust saturable absorber for ultrafast photonics [J]. ***Laser Photonics Rev***, 2020: 1900367.

[60] Shi J, Yu P, Liu F, et al. 3R MoS_2 with broken inversion symmetry: a promising ultrathin nonlinear optical Device [J]. *Adv Mater*, 2017, 29: 1701486.

[61] Quan C, Lu C, He C, et al. Band alignment of $MoTe_2/MoS_2$ nanocomposite films for enhanced nonlinear optical performance [J]. *Adv Mater Interfaces*, 2019, 6: 1801733.

[62] Tian X, Wei R, Liu M, et al. Ultrafast saturable absorption in TiS_2 induced by non-equilibrium electrons and the generation of a femtosecond mode-locked laser [J]. *Nanoscale*, 2018, 10: 9608-9615.

[63] Xie Z, Wu Y, Sun X, et al. Ultra-broadband nonlinear optical response of two-dimensional *h*-BN nanosheets and their hybrid gel glasses [J]. *Nanoscale*, 2018, 10: 4276-4283.

[64] Zhao G, Zhang F, Wu Y, et al. One-step exfoliation and hydroxylation of boron nitride nanosheets with enhanced optical limiting performance [J]. *Adv Opt Mater*, 2016, 4: 141-146.

[65] Xu Y, Jiang XF, Ge Y, et al. Size-dependent nonlinear optical properties of black phosphorus nanosheets and their applications in ultrafast photonics [J]. *J Mater Chem C*, 2017, 5: 3007-3013.

[66] Shi M, Huang S, Dong N, et al. Donor–acceptor type blends composed of black phosphorus and C_{60} for solid-state optical limiters [J]. *Chem Commun*, 2018, 54: 366-369.

[67] Wang K, Szydłowska B M, Wang G, et al. Ultrafast nonlinear excitation dynamics of black phosphorus nanosheets from visible to mid-infrared [J]. *ACS Nano*, 2016, 10: 6923-6932.

[68] Wang C, Zhang T, Lin W. Rational synthesis of noncentrosymmetric metal –organic frameworks for second-order nonlinear optics [J]. *Chem Rev*, 2012, 112: 1084-1104.

[69] Niu R J, Zhou W F, Liu Y, et al. Morphology-dependent third-order optical nonlinearity of a 2D Co-based metal –organic framework with a porphyrinic skeleton [J]. *Chem Commun*, 2019, 55: 4873-4876.

[70] Shi J m, Xu W, Liu Q y, et al. Polynitrile-bridged two-dimensional crystal: Eu(lll) complex with strong fluorescence emission and NLO property [J]. ***Chem Commun***, 2002: 756-757.

[71] Biswal B P, Valligatla S, Wang M, et al. Nonlinear optical switching in regioregular porphyrin covalent organic frameworks [J]. *Angew Chem Int Ed*, 2019, 58: 6896-6900.

[72] Dong Y, Zhang Y, Li X, et al. Chiral perovskites: promising materials toward next-generation optoelectronics [J]. *Small*, 2019, 15: 1902237.

[73] Xue J, Yang D, Cai B, et al. Photon-induced reversible phase transition in $CsPbBr_3$ perovskite [J]. *Adv Funct Mater*, 2019, 29: 1807922.

[74] Hu J, Yan L, You W. Two-dimensional organic –inorganic hybrid perovskites: a new platform for optoelectronic applications [J]. *Adv Mater*, 2018, 30: 1802041.

[75] Correa Baena J P, Saliba M, Buonassisi T, et al. Promises and challenges of perovskite solar cells [J]. *Science*, 2017, 358: 739-744.

[76] Grancini G, Nazeeruddin M K. Dimensional tailoring of hybrid perovskites for photovoltaics [J]. *Nat Rev Mater*, 2019, 4: 4-22.

[77] Li W, Wang Z, Deschler F, et al. Chemically diverse and multifunctional hybrid organic-inorganic perovskites [J]. *Nat Rev Mater*, 2017, 2: 16099.

[78] Stoumpos C C, Cao D H, Clark D J, et al. Ruddlesden-popper hybrid lead iodide perovskite 2D homologous semiconductors [J]. *Chem Mater*, 2016, 28: 2852-2867.

[79] Nazarenko O, Kotyrba MR, Yakunin S, et al. Guanidinium-formamidinium lead iodide: a layered perovskite-related compound with red luminescence at room temperature [J]. *J Am Chem Soc*, 2018, 140: 3850-3853.

[80] Koh TM, Shanmugam V, Schlipf J, et al. Nanostructuring mixed-dimensional perovskites: a route toward tunable, efficient photovoltaics [J]. *Adv Mater*, 2016, 28: 3653-3661.

[81] Saparov B, Mitzi D B. Organic-inorganic perovskites: structural versatility for functional materials design [J]. *Chem Rev*, 2016, 116: 4558-4596.

[82] Lee H-D, Kim H, Cho H, et al. Efficient ruddlesden –popper perovskite light-emitting diodes with randomly oriented nanocrystals [J]. ***Adv Funct Mater***, 2019, 29: 1901225.

[83] Zheng Y, Niu T, Ran X, et al. Unique characteristics of 2D Ruddlesden–Popper (2DRP) perovskite for future photovoltaic application [J]. *J Mater Chem A*, 2019, 7: 13860-13872.

[84] Yu S, Yan Y, Abdellah M, et al. Nonconfinement structure sevealed in Dion–Jacobson type quasi-2D perovskite expedites interlayer charge transport [J]. *Small*, 2019, 15: 1905081.

[85] Mao L, Ke W, Pedesseau L, et al. Hybrid Dion–Jacobson 2D lead iodide perovskites [J]. *J Am Chem Soc*, 2018, 140: 3775-3783.

[86] Li Y, Milić J V, Ummadisingu A, et al. Bifunctional organic spacers for formamidinium-based hybrid Dion–Jacobson two-dimensional perovskite solar cells [J]. *Nano Lett*, 2019, 19: 150-157.

[87] Zhang Y, Wang P, Tang M C, et al. Dynamical transformation of two-dimensional perovskites with alternating cations in the interlayer space for high-performance photovoltaics [J]. *J Am*

Chem Soc, 2019, 141: 2684-2694.

[88] Soe C M M, Stoumpos C C, Kepenekian M, et al. New type of 2D perovskites with alternating cations in the interlayer space, $(C(NH_2)_3)(CH_3NH_3)_nPb_nI_{3n+1}$: structure, properties, and photovoltaic performance [J]. *J Am Chem Soc*, 2017, 139: 16297-16309.

[89] Mao L, Stoumpos C C, Kanatzidis M G. Two-dimensional hybrid halide perovskites: principles and promises [J]. *J Am Chem Soc*, 2019, 141: 1171-1190.

[90] Zimmermann I, Aghazada S, Nazeeruddin M K. Lead and HTM free stable two-dimensional tin perovskites with suitable band gap for solar cell applications [J]. *Angew Chem Int Ed*, 2019, 58: 1072-1076.

[91] Li X, Hoffman J, Ke W, et al. Two-dimensional halide perovskites incorporating straight chain symmetric diammonium ions, $(NH_3C_mH_{2m}NH_3)(CH_3NH_3)_{n-1}Pb_nI_{3n+1}$ (m = 4–9; n = 1–4) [J]. *J Am Chem Soc*, 2018, 140: 12226-12238.

[92] Kim H, Huynh K A, Kim S Y, et al. 2D and quasi-2D halide perovskites: applications and progress [J]. ***Phys Status Solidi RRL***, 2019, 14: 1900435.

[93] Wang N, Cheng L, Ge R, et al. Perovskite light-emitting diodes based on solution-processed self-organized multiple quantum wells [J]. *Nat Photonics*, 2016, 10: 699-704.

[94] Yuan M, Quan LN, Comin R, et al. Perovskite energy funnels for efficient light-emitting diodes [J]. *Nat Nanotechnol*, 2016, 11: 872.

[95] Chen Z, Guo Y, Wertz E, et al . Merits and challenges of ruddlesden–popper soft halide perovskites in electro-optics and optoelectronics [J]. *Adv Mater*, 2019, 31: 1803514.

[96] Yuan Z, Shu Y, Xin Y, et al. Highly luminescent nanoscale quasi-2D layered lead bromide perovskites with tunable emissions [J]. *Chem Commun*, 2016, 52: 3887-3890.

[97] Mao L, Guo P, Kepenekian M, et al. Structural diversity in white-light-emitting hybrid lead bromide perovskites [J]. *J Am Chem Soc*, 2018, 140: 13078-13088.

[98] Zhou L, Liao J F, Huang Z G, et al. Intrinsic self-trapped emission in 0D lead-free $(C_4H_{14}N_2)_2In_2Br_{10}$ single crystal [J]. *Angew Chem Int Ed*, 2019, 58: 15435-15440.

[99] Cortecchia D, Neutzner S, Srimath Kandada A R, et al. Broadband emission in two-dimensional hybrid perovskites: the role of structural deformation [J]. *J Am Chem Soc*, 2017, 139: 39-42.

[100] Jung M H. White-light emission from the structural distortion induced by control of halide composition of two-dimensional perovskites ($(C_6H_5CH_2NH_3)_2PbBr_{4-x}Cl_x$) [J]. *Inorg Chem*, 2019, 58: 6748-6757.

[101] Zhang L, Wu L, Wang K, et al. Pressure-induced broadband emission of 2D organic-inorganic hybrid perovskite $(C_6H_5C_2H_4NH_3)_2PbBr_4$ [J]. *Adv Sci*, 2019, 6: 1801628.

[102] Li X, Guo P, Kepenekian M, et al. Small cyclic diammonium cation templated (110)-oriented 2D halide (X = I, Br, Cl) perovskites with white-light emission [J]. *Chem Mater*, 2019, 31: 3582-3590.

[103] Mitzi D B, Wang S, Feild C A, et al. Conducting layered organic-inorganic halides containing <110>-oriented perovskite sheets [J]. *Science*, 1995, 267: 1473-1476.

[104] Mao L, Wu Y, Stoumpos C C, et al. White-light emission and structural distortion in new corrugated two-dimensional lead bromide perovskites [J]. *J Am Chem Soc*, 2017, 139: 5210-5215.

[105] Li Y Y, Lin C K, Zheng G L, et al. Novel <110>-oriented organic−inorganic perovskite compound stabilized by *n*-(3-aminopropyl)imidazole with improved optical properties [J]. *Chem Mater*, 2006, 18: 3463-3469.

[106] Cortecchia D, Yin J, Petrozza A, et al. White light emission in low-dimensional perovskites [J]. *J Mater Chem C*, 2019, 7: 4956-4969.

[107] Wu Z, Ji C, Sun Z, et al. Broadband white-light emission with a high color rendering index in a two-dimensional organic-inorganic hybrid perovskite [J]. ***J Mater Chem C***, 2018, 6: 1171-1175.

[108] Booker E P, Thomas T H, Quarti C, et al. Formation of long-lived color centers for broadband visible light emission in low-dimensional layered perovskites [J]. *J Am Chem Soc*, 2017, 139: 18632-18639.

[109] McCall K M, Stoumpos C C, Kontsevoi O Y, et al. From 0D $Cs_3Bi_2I_9$ to 2D $Cs_3Bi_2I_6Cl_3$: dimensional expansion induces a direct band gap but enhances electron–phonon coupling [J]. *Chem Mater*, 2019, 31: 2644-2650.

[110] Jiang F, Yang D, Jiang Y, et al. Chlorine-incorporation-induced formation of the layered phase for antimony-based lead-free perovskite solar cells [J]. *J Am Chem Soc*, 2018, 140: 1019-1027.

[111] Liu Z, Zhao X, Zunger A, et al. Design of mixed-cation tri-layered Pb-free halide perovskites for optoelectronic applications [J]. *Adv Electron Mater*, 2019, 5: 1900234.

[112] Vargas B, Ramos E, Pérez-Gutiérrez E, et al. A direct bandgap copper–antimony halide perovskite [J]. *J Am Chem Soc*, 2017, 139: 9116-9119.

[113] Chai S, Xiong J, Zheng Y, et al. Dielectric phase transition of

an A_2BX_4-type perovskite with a pentahedral to octahedral transformation [J]. ***Dalton Trans***, 2020, 49: 2218-2224.

[114] Shi E, Gao Y, Finkenauer B P, et al. Two-dimensional halide perovskite nanomaterials and heterostructures [J]. ***Chem Soc Rev***, 2018, 47: 6046-6072.

[115] Huo C, Cai B, Yuan Z, et al. Two-dimensional metal halide perovskites: theory, synthesis, and optoelectronics [J]. ***Small Methods***, 2017, 1: 1600018.

[116] Wang J, Shen H, Li W, et al. The role of chloride incorporation in lead-free 2D perovskite $(BA)_2SnI_4$: morphology, photoluminescence, phase transition, and charge transport [J]. ***Adv Sci***, 2019, 6: 1802019.

[117] Hwang B, Lee J S. 2D perovskite-based self-aligned lateral heterostructure photodetectors utilizing vapor deposition [J]. ***Adv Opt Mater***, 2019, 7: 1801356.

[118] Chen J, Wang Y, Gan L, et al. Generalized self-doping engineering towards ultrathin and large-sized two-dimensional homologous perovskites [J]. ***Angew Chem Int Ed***, 2017, 56: 14893-14897.

[119] Chen Z, Wang Y, Sun X, et al. Remote phononic effects in epitaxial Ruddlesden –Popper halide perovskites [J]. ***J Phys Chem Lett***, 2018, 9: 6676-6682.

[120] Milot R L, Sutton R J, Eperon G E, et al. Charge-carrier dynamics in 2D hybrid metal–halide perovskites [J]. ***Nano Lett***, 2016, 16: 7001-7007.

[121] Li J, Wang J, Ma J, et al. Self-trapped state enabled filterless narrowband photodetections in 2D layered perovskite single crystals [J]. ***Nat Commun***, 2019, 10: 806.

[122] Li H, Lu J, Zhang T, et al. Cation-assisted restraint of a wide quantum well and interfacial charge accumulation in two-dimensional perovskites [J]. ***ACS Energy Lett***, 2018, 3: 1815-1823.

[123] Guo R, Zhu Z, Boulesbaa A, et al. Synthesis and photoluminescence properties of 2D phenethylammonium lead bromide perovskite nanocrystals [J]. ***Small Methods***, 2017, 1: 1700245.

[124] Fang H H, Adjokatse S, Shao S, et al. Long-lived hot-carrier light emission and large blue shift in formamidinium tin triiodide perovskites [J]. ***Nat Commun***, 2018, 9: 243.

[125] Long G, Jiang C, Sabatini R, et al. Spin control in reduced-dimensional chiral perovskites [J]. ***Nat Photonics***, 2018, 12: 528-533.

[126] Guan J, Zhang C, Gao D, et al. Drastic photoluminescence modulation of an organic molecular crystal with high pressure [J]. ***Mater Chem Front***, 2019, 3: 1510-1517.

[127] Smith M D, Karunadasa H I. White-light emission from layered halide perovskites [J]. ***Acc Chem Res***, 2018, 51: 619-627.

[128] Aharon S, Etgar L. Two dimensional organometal halide perovskite nanorods with tunable optical properties [J]. ***Nano Lett***, 2016, 16: 3230-3235.

[129] Cao Y, Wang N, Tian H, et al. Perovskite light-emitting diodes based on spontaneously formed submicrometre-scale structures [J]. ***Nature***, 2018, 562: 249-253.

[130] Lee J W, Dai Z, Han T H, et al. 2D perovskite stabilized phase-pure formamidinium perovskite solar cells [J]. ***Nat Commun***, 2018, 9: 3021.

[131] Cao D H, Stoumpos C C, Yokoyama T, et al. Thin films and solar cells based on semiconducting two-dimensional Ruddlesden-Popper $(CH_3(CH_2)_3NH_3)_2(CH_3NH_3)_{n-1}Sn_nI_{3n+1}$ perovskites [J]. ***ACS Energy Lett***, 2017, 2: 982-990.

[132] Chen Q, Wu J, Ou X, et al. All-inorganic perovskite nanocrystal scintillators [J]. ***Nature***, 2018, 561: 88-93.

[133] Wang J, Li J, Lan S, et al. Controllable growth of centimeter-sized 2D perovskite heterostructures for highly narrow dual-band photodetectors [J]. ***ACS Nano***, 2019, 13: 5473-5484.

[134] Dohner E R, Jaffe A, Bradshaw L R, et al. Intrinsic white-light emission from layered hybrid perovskites [J]. ***J Am Chem Soc***, 2014, 136: 13154-13157.

[135] Thouin F, Valverde-Chávez D A, Quarti C, et al. Phonon coherences reveal the polaronic character of excitons in two-dimensional lead halide perovskites [J]. ***Nat Mater***, 2019, 18: 349-356.

[136] Yangui A, Garrot D, Lauret J S, et al. Optical investigation of broadband white-light emission in self-assembled organic-inorganic perovskite $(C_6H_{11}NH_3)_2PbBr_4$ [J]. ***J Phys Chem C***, 2015, 119: 23638-23647.

[137] Thirumal K, Chong W K, Xie W, et al. Morphology-independent stable white-light emission from self-assembled two-dimensional perovskites driven by strong exciton–phonon coupling to the organic framework [J]. ***Chem Mater***, 2017, 29: 3947-3953.

[138] Mao L, Wu Y, Stoumpos C C, et al. Tunable white-light emission in single-cation-templated three-layered 2D perovskites $(CH_3CH_2NH_3)_4Pb_3Br_{10-x}Cl_x$ [J]. ***J Am Chem Soc***, 2017, 139: 11956-11963.

[139] Ji C, Wang S, Li L, et al. The first 2D hybrid perovskite ferroelectric showing broadband white-light emission with high color rendering index [J]. ***Adv Funct Mater***, 2019, 29: 1805038.

[140] Huang B, Chen W C, Li Z, et al. Manipulation of molecular

aggregation states to realize polymorphism, AIE, MCL, and TADF in a single molecule [J]. *Angew Chem Int Ed*, 2018, 57: 12473-12477.

[141] Zhang Y L, Ran Q, Wang Q, et al. High-efficiency red organic light-emitting diodes with external quantum efficiency close to 30% based on a novel thermally activated delayed fluorescence emitter [J]. *Adv Mater*, 2019, 31: 1902368.

[142] Hu H, Meier F, Zhao D, et al. Efficient room-temperature phosphorescence from organic–inorganic hybrid perovskites by molecular engineering [J]. *Adv Mater*, 2018, 30: 1707621.

[143] An Z, Zheng C, Tao Y, et al. Stabilizing triplet excited states for ultralong organic phosphorescence [J]. *Nat Mater*, 2015, 14: 685.

[144] Ben Haj Salah M, Mercier N, Allain M, et al. Dual phosphorescence from the organic and inorganic moieties of 1D hybrid perovskites of the $Pb_{n'}Br_{4n'+2}$ series (n' = 2, 3, 4, 5) [J]. *J Mater Chem C*, 2019, 7: 4424-4433.

[145] Bolton O, Lee K, Kim H J, et al. Activating efficient phosphorescence from purely organic materials by crystal design [J]. *Nat Chem*, 2011, 3: 205-210.

[146] Zheng H, Liu G, Zhu L, et al. The effect of hydrophobicity of ammonium salts on stability of quasi-2D perovskite materials in moist condition [J]. *Adv Energy Mater*, 2018, 8: 1800051.

[147] Ding C, Zhang Y, Liu F, et al. Effect of the conduction band offset on interfacial recombination behavior of the planar perovskite solar cells [J]. *Nano Energy*, 2018, 53: 17-26.

[148] Yuan C, Li X, Semin S, et al. Chiral lead halide perovskite nanowires for second-order nonlinear optics [J]. *Nano Lett*, 2018, 18: 5411-5417.

[149] Wang J, Fang C, Ma J, et al. Aqueous synthesis of low-dimensional lead halide perovskites for room-temperature circularly polarized light emission and detection [J]. *ACS Nano*, 2019, 13: 9473-9481.

[150] Xing C, Huang W, Xie Z, et al. Ultrasmall bismuth quantum dots: facile liquid-phase exfoliation, characterization, and application in high-performance UV –Vis photodetector [J]. *ACS Photonics*, 2018, 5: 621-629.

[151] Xie Z, Xing C, Huang W, et al. Ultrathin 2D nonlayered tellurium nanosheets: facile liquid-phase exfoliation, characterization, and photoresponse with high performance and enhanced stability [J]. *Adv Funct Mater*, 2018, 28: 1705833.

[152] Fan T, Xie Z, Huang W, et al. Two-dimensional non-layered selenium nanoflakes: facile fabrications and applications for self-powered photo-detector [J]. *Nanotechnology*, 2019, 30: 114002.

[153] Huang W, Xie Z, Fan T, et al. Black-phosphorus-analogue tin monosulfide: an emerging optoelectronic two-dimensional material for high-performance photodetection with improved stability under ambient/harsh conditions [J]. *J Mater Chem C*, 2018, 6: 9582-9593.

[154] Huang L, Dong B, Guo X, et al. Waveguide-integrated black phosphorus photodetector for mid-infrared applications [J]. *ACS Nano*, 2019, 13: 913-921.

[155] Brenner T M, Egger D A, Kronik L, et al. Hybrid organic—inorganic perovskites: low-cost semiconductors with intriguing charge-transport properties [J]. *Nat Rev Mater*, 2016, 1: 15007.

[156] Qi X, Zhang Y, Ou Q, et al. Photonics and optoelectronics of 2D metal-halide perovskites [J]. *Small*, 2018, 14: 1800682.

[157] Zhang Y, Liu Y, Xu Z, et al. Two-dimensional $(PEA)_2PbBr_4$ perovskite single crystals for a high performance UV-detector [J]. *J Mater Chem C*, 2019, 7: 1584-1591.

[158] Li L, Sun Z, Wang P, et al. Tailored engineering of an unusual $(C_4H_9NH_3)_2(CH_3NH_3)_2Pb_3Br_{10}$ two-dimensional multilayered perovskite ferroelectric for a high-performance photodetector [J]. *Angew Chem Int Ed*, 2017, 56: 12150-12154.

[159] Tan Z, Wu Y, Hong H, et al. Two-dimensional $(C_4H_9NH_3)_2PbBr_4$ perovskite crystals for high-performance photodetector [J]. *J Am Chem Soc*, 2016, 138: 16612-16615.

[160] Qian L, Sun Y, Sun M, et al. 2D perovskite microsheets for high-performance photodetectors [J]. ***J Mater Chem C***, 2019, 7: 5353-5358.

[161] Xie Z, Zhang F, Liang Z, et al. Revealing of the ultrafast third-order nonlinear optical response and enabled photonic application in two-dimensional tin sulfide [J]. *Photon Res*, 2019, 7: 494-502.

[162] Wu L, Xie Z, Lu L, et al. Few-layer tin sulfide: a promising black-phosphorus-analogue 2D material with exceptionally large nonlinear optical response, high stability, and applications in all-optical switching and wavelength conversion [J]. *Adv Opt Mater*, 2018, 6: 1700985.

[163] Xing C, Xie Z, Liang Z, et al. 2D nonlayered selenium nanosheets: facile synthesis, photoluminescence, and ultrafast photonics [J]. *Adv Opt Mater*, 2017, 5: 1700884.

[164] Dean J J, van Driel H M. Graphene and few-layer graphite probed by second-harmonic generation: theory and experiment [J]. *Phys Rev B*, 2010, 82: 125411.

[165] Liu Y, Gao P, Zhang T, et al. Azide passivation of black phosphorus nanosheets: covalent functionalization affords ambient stability enhancement [J]. *Angew Chem Int Ed*, 2019,

58: 1479-1483.

[166] Szydłowska B M, Tywoniuk B, Blau W J. Size-dependent nonlinear optical response of black phosphorus liquid phase exfoliated nanosheets in nanosecond regime [J]. ***ACS Photonics***, 2018, 5: 3608-3612.

[167] Ma W, Lu J, Wan B, et al. Piezoelectricity in multilayer black phosphorus for piezotronics and nanogenerators [J]. ***Adv Mater***, 2020, 32: 1905795.

[168] Skelton J M, Burton L A, Oba F, et al. Chemical and lattice stability of the tin sulfides [J]. ***J Phys Chem C***, 2017, 121: 6446-6454.

[169] Xin C, Zheng J, Su Y, et al. Few-layer tin sulfide: a new black-phosphorus-analogue 2D material with a sizeable band gap, odd –even quantum confinement effect, and high carrier mobility [J]. ***J Phys Chem C***, 2016, 120: 22663-22669.

[170] Sarkar A S, Mushtaq A, Kushavah D, et al. Liquid exfoliation of electronic grade ultrathin tin(II) sulfide (SnS) with intriguing optical response [J]. ***npj 2D Mater Appl***, 2020, 4: 1.

[171] Wang H, Qian X. Giant optical second harmonic generation in two-dimensional multiferroics [J]. ***Nano Lett***, 2017, 17: 5027-5034.

[172] Ferrando A, Martínez Pastor J P, Suárez I. Toward metal halide perovskite nonlinear photonics [J]. ***J Phys Chem Lett***, 2018, 9: 5612-5623.

[173] Dong R, Zhang T, Feng X. Interface-assisted synthesis of 2D materials: trend and challenges [J]. ***Chem Rev***, 2018, 118: 6189-6235.

[174] Geng D, Yang H Y. Recent advances in growth of novel 2D materials: beyond graphene and transition metal dichalcogenides [J]. ***Adv Mater***, 2018, 30: 1800865.

[175] Lukatskaya M R, Mashtalir O, Ren C E, et al. Cation intercalation and high volumetric capacitance of two-dimensional titanium carbide [J]. ***Science***, 2013, 341: 1502-1505.

[176] Lim D, Suh H, Suryawanshi M, et al. Kinetically controlled growth of phase-pure SnS absorbers for thin film solar cells: achieving efficiency near 3% with long-term stability using an SnS/CdS heterojunction [J]. ***Adv Energy Mater***, 2018, 8: 1702605.

[177] Franken P A, Hill A E, Peters C W, et al. Generation of optical harmonics [J]. ***Phys Rev Lett***, 1961, 7: 118-119.

[178] Duan Y, Ju C, Yang G, et al. Aggregation induced enhancement of linear and nonlinear optical emission from a hexaphenylene derivative [J]. ***Adv Funct Mater***, 2016, 26: 8968-8977.

[179] Xu J, Semin S, Niedzialek D, et al. Self-assembled organic microfibers for nonlinear optics [J]. ***Adv Mater***, 2013, 25: 2084-2089.

[180] Chervy T, Xu J, Duan Y, et al. High-efficiency second-harmonic generation from hybrid light-matter states [J]. ***Nano Lett***, 2016, 16: 7352-7356.

[181] Boyd R W, Masters B R. Nonlinear optics, third edition [J]. ***Journal of Biomedical Optics***, 2009, 14(2): 029902.

[182] Timurdogan E, Poulton C V, Byrd M J, et al. Electric field-induced second-order nonlinear optical effects in silicon waveguides [J]. ***Nat Photonics***, 2017, 11: 200-206.

[183] Xu J, Semin S, Cremers J, et al. Controlling microsized polymorphic architectures with distinct linear and nonlinear optical properties [J]. ***Adv Opt Mater***, 2015, 3: 948-956.

[184] Xiong J, Li X, Yuan C, et al. Wavelength dependent nonlinear optical response of tetraphenylethene aggregation-induced emission luminogens [J]. ***Mater Chem Front***, 2018, 2: 2263-2271.

[185] Wang S, Yao Y, Kong J, et al. Highly efficient white-light emission in a polar two-dimensional hybrid perovskite [J]. ***Chem Commun***, 2018, 54: 4053-4056.

[186] Shi P P, Tang Y Y, Li P F, et al. Symmetry breaking in molecular ferroelectrics [J]. ***Chem Soc Rev***, 2016, 45: 3811-3827.

[187] Qin J, Huang F, Li X, et al. Enhanced second harmonic generation from ferroelectric HfO_2-based hybrid metasurfaces [J]. ***ACS Nano***, 2019, 13: 1213-1222.

[188] Liao W Q, Zhang Y, Hu C L, et al. A lead-halide perovskite molecular ferroelectric semiconductor [J]. ***Nat Commun***, 2015, 6: 7338.

[189] Wu Z, Ji C, Li L, et al. Alloying *n*-butylamine into $CsPbBr_3$ to give a two-dimensional bilayered perovskite ferroelectric material [J]. ***Angew Chem Int Ed***, 2018, 57: 8140-8143.

[190] Tang Y Y, Li P F, Liao W Q, et al. Multiaxial molecular ferroelectric thin films bring light to practical applications [J]. ***J Am Chem Soc***, 2018, 140: 8051-8059.

[191] Li L, Liu X, Li Y, et al. Two-dimensional hybrid perovskite-type ferroelectric for highly polarization-sensitive shortwave photodetection [J]. ***J Am Chem Soc***, 2019, 141: 2623-2629.

[192] Han S, Liu X, Liu Y, et al. High-temperature antiferroelectric of lead iodide hybrid perovskites [J]. ***J Am Chem Soc***, 2019, 141: 12470-12474.

[193] Liu C, Mei D, Cao W, et al. Mn-based tin sulfide $Sr_3MnSn_2S_8$ with a wide band gap and strong nonlinear optical response [J]. ***J Mater Chem C***, 2019, 7: 1146-1150.

[194] Ding F, Nisbet M L, Yu H, et al. Syntheses, structures, and properties of non-centrosymmetric quaternary tellurates $BiMTeO_6$ (M = Al, Ga) [J]. ***Inorg Chem***, 2018, 57: 7950-7956.

[195] Chen J, Hu C L, Mao F F, et al. A facile route to nonlinear optical materials: three-site aliovalent substitution involving one cation and two anions [J]. ***Angew Chem Int Ed***, 2019, 58: 2098-2102.

[196] Strayer M E, Gupta A S, Akamatsu H, et al. Emergent noncentrosymmetry and piezoelectricity driven by oxygen octahedral rotations in n = 2 Dion –Jacobson phase layer perovskites [J]. ***Adv Funct Mater***, 2016, 26: 1930-1937.

[197] Kim H G, Tran T T, Choi W, et al. Two new non-centrosymmetric n = 3 layered Dion-Jacobson perovskites: polar $RbBi_2Ti_2NbO_{10}$ and nonpolar $CsBi_2Ti_2TaO_{10}$ [J]. ***Chem Mater***, 2016, 28: 2424-2432.

[198] Gupta A S, Akamatsu H, Strayer M E, et al. Improper inversion symmetry breaking and piezoelectricity through oxygen octahedral rotations in layered perovskite family, Li$R$$TiO_4$ (R = rare earths) [J]. ***Adv Electron Mater***, 2016, 2: 1500196.

[199] Wei W J, Jiang X X, Dong L Y, et al. Regulating second-harmonic generation by van der Waals interactions in two-dimensional lead halide perovskite nanosheets [J]. ***J Am Chem Soc***, 2019, 141: 9134-9139.

[200] Yang C K, Chen W N, Ding Y T, et al. The first 2D homochiral lead iodide perovskite ferroelectrics:[R-and S-1-(4-chloro-phenyl)ethylammonium]$_2PbI_4$ [J]. ***Adv Mater***, 2019, 31: 1808088.

[201] Savoini M, Huber L, Cuppen H, et al. THz generation and detection by fluorenone based organic crystals [J]. ***ACS Photonics***, 2018, 5: 671-677.

[202] Maysonnave J, Huppert S, Wang F, et al. Terahertz generation by dynamical photon drag effect in graphene excited by femtosecond optical pulses [J]. ***Nano Lett***, 2014, 14: 5797-5802.

[203] Chanana A, Zhai Y, Baniya S, et al. Colour selective control of terahertz radiation using two-dimensional hybrid organic inorganic lead-trihalide perovskites [J]. ***Nat Commun***, 2017, 8: 1328.

[204] Weis P, Garcia-Pomar J L, Hh M, et al. Spectrally wide-band terahertz wave modulator based on optically tuned graphene [J]. ***ACS Nano***, 2012, 6: 9118-9124.

[205] Haynes A S, Saouma F O, Otieno C O, et al. Phase-change behavior and nonlinear optical second and third harmonic generation of the one-dimensional $K_{(1-x)}Cs_xPSe_6$ and metastable β-$CsPSe_6$ [J]. ***Chem Mater***, 2015, 27: 1837-1846.

[206] Deckers S, Steverlynck J, Willot P, et al. Regioregularity increases second-order nonlinear optical response of polythiophenes in solution [J]. ***J Phys Chem C***, 2015, 119: 18513-18517.

[207] Saouma F O, Stoumpos C C, Wong J, et al. Selective enhancement of optical nonlinearity in two-dimensional organic-inorganic lead iodide perovskites [J]. ***Nat Commun***, 2017, 8: 742.

[208] Hanamura E, Nagaosa N, Kumagai M, et al. Quantum wells with enhanced exciton effects and optical non-linearity [J]. ***Mater Sci Eng, B***, 1988, 1: 255-258.

[209] Abdelwahab I, Grinblat G, Leng K, et al. Highly enhanced third-harmonic generation in 2D perovskites at excitonic resonances [J]. ***ACS Nano***, 2018, 12: 644-650.

[210] Youngblood N, Peng R, Nemilentsau A, et al. Layer-tunable third-harmonic generation in multilayer black phosphorus [J]. ***ACS Photonics***, 2017, 4: 8-14.

[211] Wei Z, Guo D, Thieme J, et al. The importance of relativistic effects on two-photon absorption spectra in metal halide perovskites [J]. ***Nat Commun***, 2019, 10: 5342.

[212] Zhou F, Abdelwahab I, Leng K, et al. 2D perovskites with giant excitonic optical nonlinearities for high-performance sub-bandgap photodetection [J]. ***Adv Mater***, 2019, 31: 1904155.

[213] Zhang W F, Huang Y B, Zhang M S. Optical properties of ferroelectric (Pb, La)(Zr, Ti)O_3 thin films grown by pulsed laser deposition [J]. ***Appl Surf Sci***, 2000, 158: 185-189.

[214] Liu W, Li X, Song Y, et al. Cooperative enhancement of two-photon-absorption-induced photoluminescence from a 2D perovskite-microsphere hybrid dielectric structure [J]. ***Adv Funct Mater***, 2018, 28: 1707550.

[215] Wang J, Mi Y, Gao X, et al. Giant nonlinear optical response in 2D perovskite heterostructures [J]. ***Adv Opt Mater***, 2019, 7: 1900398.

[216] Wang L, Li W, Li M, et al. Ultrastable amine, sulfo cofunctionalized graphene quantum dots with high two-photon fluorescence for cellular imaging [J]. ***ACS Sustainable Chem Eng***, 2018, 6: 4711-4716.

[217] Zhu X, Xu H, Liu Y, et al. Two-photon up-conversion photoluminescence realized through spatially extended gap states in quasi-2D perovskite films [J]. ***Adv Mater***, 2019, 31: 1901240.

[218] Saouma F O, Stoumpos C C, Kanatzidis M G, et al. Multiphoton absorption order of $CsPbBr_3$ as determined by wavelength-dependent nonlinear optical spectroscopy [J]. ***J Phys Chem Lett***, 2017, 8: 4912-4917.

[219] Sharma D, Malik BP, Gaur A. Two and four photon absorption and nonlinear refraction in undoped, chromium doped and copper doped ZnS quantum dots [J]. ***J Phys Chem Solids***, 2015, 87: 163-170.

[220] Friese D H, Bast R, Ruud K. Five-photon absorption and selective enhancement of multiphoton absorption processes [J]. ***ACS Photonics***, 2015, 2: 572-577.

[221] Xiang J, Cai X, Lou X, et al. Biocompatible green and red fluorescent organic dots with remarkably large two-photon action cross sections for targeted cellular imaging and real-time intravital blood vascular visualization [J]. ***ACS Appl Mater Interfaces***, 2015, 7: 14965-14974.

[222] Feng R, Sun Y, Tian M, et al. A membrane-permeable dye for living cells with large two-photon excited fluorescence action cross-sections for bioimaging [J]. ***J Mater Chem B***, 2015, 3: 8644-8649.

[223] Horton N G, Wang K, Kobat D, et al. In vivo three-photon microscopy of subcortical structures within an intact mouse brain [J]. ***Nat Photonics***, 2013, 7: 205-209.

[224] Mushtaq A, Kushavah D, Ghosh S, et al. Nonlinear optical properties of benzylamine lead(II) bromide perovskite microdisks in femtosecond regime [J]. ***Appl Phys Lett***, 2019, 114: 051902.

[225] Manzi A, Tong Y, Feucht J, et al. Resonantly enhanced multiple exciton generation through below-band-gap multi-photon absorption in perovskite nanocrystals [J]. ***Nat Commun***, 2018, 9: 1518.

[226] Lu S, Zhou F, Zhang Q, et al. Layered hybrid perovskites for highly efficient three-photon absorbers: theory and experimental observation [J]. ***Adv Sci***, 2019, 6: 1801626.

[227] Chen W, Bhaumik S, Veldhuis S A, et al. Giant five-photon absorption from multidimensional core-shell halide perovskite colloidal nanocrystals [J]. ***Nat Commun***, 2017, 8: 15198.

[228] Bhaumik S, Veldhuis S A, Ng Y F, et al. Highly stable, luminescent core-shell type methylammonium-octylammonium lead bromide layered perovskite nanoparticles [J]. ***Chem Commun***, 2016, 52: 7118-7121.

[229] Zhu B H, Zhang H C, Zhang J Y, et al. Surface-related two-photon absorption and refraction of CdSe quantum dots [J]. ***Appl Phys Lett***, 2011, 99: 021908.

[230] Zhu B H, Zhang H C, Zhang Z Y, et al. Effect of shell thickness on two-photon absorption and refraction of colloidal CdSe/CdS core/shell nanocrystals [J]. ***Appl Phys Lett***, 2011, 99: 231903.

[231] Zheng Q, Zhu H, Chen S C, et al. Frequency-upconverted stimulated emission by simultaneous five-photon absorption [J]. ***Nat Photonics***, 2013, 7: 234-239.

[232] Chen H, Wang F, Liu M, et al. Near-infrared broadband polymer-dot modulator with high optical nonlinearity for ultrafast pulsed lasers [J]. ***Laser Photonics Rev***, 2019, 13: 1800326.

[233] Li P, Chen Y, Yang T, et al. Two-dimensional $CH_3NH_3PbI_3$ perovskite nanosheets for ultrafast pulsed fiber lasers [J]. ***ACS Appl Mater Interfaces***, 2017, 9: 12759-12765.

[234] Hong S, Lédée F, Park J, et al. Mode-locking of all-fiber lasers operating at both anomalous and normal dispersion regimes in the C-and L-bands using thin film of 2D perovskite crystallites [J]. ***Laser Photonics Rev***, 2018, 12: 1800118.

[235] Zhang H, Liao Q, Wu Y, et al. Two-dimensional Ruddlesden–Popper perovskites microring laser array [J]. ***Adv Mater***, 2018, 30: 1706186.

[236] Gu Z, Wang K, Sun W, et al. Two-photon pumped $CH_3NH_3PbBr_3$ perovskite microwire lasers [J]. ***Adv Opt Mater***, 2016, 4: 472-479.

[237] Wei Q, Du B, Wu B, et al. Two-photon optical properties in individual organic-inorganic perovskite microplates [J]. ***Adv Opt Mater***, 2017, 5: 1700809.

[238] Zhang Y, Lim C-K, Dai Z, et al. Photonics and optoelectronics using nano-structured hybrid perovskite media and their optical cavities [J]. ***Phys Rep***, 2019, 795: 1-51.

[239] Yu H, Peng Y, Yang Y, et al. Plasmon-enhanced light–matter interactions and applications [J]. ***npj Comput Mater***, 2019, 5: 45.

[240] Shang Q, Zhang S, Liu Z, et al. Surface plasmon enhanced strong exciton –photon coupling in hybrid inorganic –organic perovskite nanowires [J]. ***Nano Lett***, 2018, 18: 3335-3343.

[241] Kauranen M, Zayats A V. Nonlinear plasmonics [J]. ***Nat Photonics***, 2012, 6: 737-748.

[242] Xie Z, Duo Y, Lin Z, et al. The rise of 2D photothermal materials beyond graphene for clean water production [J]. ***Adv Sci***, 2020, 7: 1902236.

[243] Xie Z, Wang D, Fan T, et al. Black phosphorus analogue tin sulfide nanosheets: synthesis and application as near-infrared photothermal agents and drug delivery platforms for cancer therapy [J]. ***J Mater Chem B***, 2018, 6: 4747-4755.

[244] Chen J, Fan T, Xie Z, et al. Advances in nanomaterials for photodynamic therapy applications: Status and challenges [J]. ***Biomaterials***, 2020, 237: 119827.